AGU PUBLICATIONS

JGR

Journal of Geophysical Research: Atmospheres

RESEARCH ARTICLE
10.1002/2015JD023465

Foehn winds link climate-driven warming to ice shelf evolution in Antarctica

M. R. Cape[1,2], Maria Vernet[1], Pedro Skvarca[3], Sebastián Marinsek[4], Ted Scambos[5], and Eugene Domack[6]

[1]Scripps Institution of Oceanography, University of California, San Diego, California, USA, [2]Woods Hole Oceanographic Institution, Falmouth, Massachusetts, USA, [3]Glaciarium, Museo del Hielo Patagónico, El Calafate, Argentina, [4]Instituto Antártico Argentino, Buenos Aires, Argentina, [5]National Snow and Ice Data Center, Boulder, Colorado, USA, [6]College of Marine Science, University of South Florida, St. Petersburg, Florida, USA

Key Points:
- Foehn winds increase regional temperature along the Antarctic Peninsula
- Variability in foehn wind frequency is linked to the Southern Annular Mode
- Westerly wind events contribute to glacial melt

Supporting Information:
- Figures S1–S11

Correspondence to:
M. R. Cape,
mcape@whoi.edu

Citation:
Cape, M. R., M. Vernet, P. Skvarca, S. Marinsek, T. Scambos, and E. Domack (2015), Foehn winds link climate-driven warming to ice shelf evolution in Antarctica, *J. Geophys. Res. Atmos.*, *120*, 11,037–11,057, doi:10.1002/2015JD023465.

Received 3 APR 2015
Accepted 2 OCT 2015
Accepted article online 5 OCT 2015
Published online 3 NOV 2015

Abstract Rapid warming of the Antarctic Peninsula over the past several decades has led to extensive surface melting on its eastern side, and the disintegration of the Prince Gustav, Larsen A, and Larsen B ice shelves. The warming trend has been attributed to strengthening of circumpolar westerlies resulting from a positive trend in the Southern Annular Mode (SAM), which is thought to promote more frequent warm, dry, downsloping foehn winds along the lee, or eastern side, of the peninsula. We examined variability in foehn frequency and its relationship to temperature and patterns of synoptic-scale circulation using a multidecadal meteorological record from the Argentine station Matienzo, located between the Larsen A and B embayments. This record was further augmented with a network of six weather stations installed under the U.S. NSF LARsen Ice Shelf System, Antarctica, project. Significant warming was observed in all seasons at Matienzo, with the largest seasonal increase occurring in austral winter (+3.71°C between 1962–1972 and 1999–2010). Frequency and duration of foehn events were found to strongly influence regional temperature variability over hourly to seasonal time scales. Surface temperature and foehn winds were also sensitive to climate variability, with both variables exhibiting strong, positive correlations with the SAM index. Concomitant positive trends in foehn frequency, temperature, and SAM are present during austral summer, with sustained foehn events consistently associated with surface melting across the ice sheet and ice shelves. These observations support the notion that increased foehn frequency played a critical role in precipitating the collapse of the Larsen B ice shelf.

1. Introduction

Observations (often discontinuous) from sparse meteorological stations collected over the last six decades have shown a dramatic increase in near-surface temperature along the Antarctic Peninsula (AP), with rates exceeding those observed both regionally and globally [*Vaughan et al.*, 2003; *Bromwich et al.*, 2013]. This trend is part of a greater and ongoing change in surface conditions across much of West Antarctica [*Kwok and Comiso*, 2002; *Steig et al.*, 2009; *Nicolas and Bromwich*, 2014]. Warming across the AP is, however, not spatially uniform, with some of the strongest statistical trends occurring over the eastern side of the peninsula [*Marshall et al.*, 2006]. Climatologically, the narrow mountain chain of the AP separates a warm, maritime climate along the western coastline from a cold continental climate to the east, leading to an average 5–10°C climatological temperature difference at similar latitude across the barrier [*Martin and Peel*, 1978; *King and Turner*, 2009; *Cook and Vaughan*, 2010]. Yet in recent years, rapid atmospheric warming along the eastern AP has led to major changes in regional climate and ice conditions across the land-ocean continuum, including higher rates of seasonal surface melting on the Larsen A and B ice shelves [*Skvarca et al.*, 1999a; *Scambos et al.*, 2003; *van den Broeke*, 2005]. This pattern of increased melt over the ice shelves is also part of a larger trend toward higher temperature and melt over the NW Weddell Sea since the late 1940s, which significantly intensified since the 1950s [*Abram et al.*, 2013]. The propagation of glacial crevasses caused by the higher surface temperatures and the accumulated meltwater load is thought to have ultimately caused the retreat and structural collapse of these ice shelves in 1995 and 2002 [*Scambos et al.*, 2000, 2009], precipitating changes among the cryosphere, ocean, ecosystem, and deposystem [*Gutt et al.*, 2011; *Rignot et al.*, 2004; *Scambos et al.*, 2004; *Cape et al.*, 2014; *Rebesco et al.*, 2014].

Marshall et al. [2006] linked the rapid rise in temperature along the eastern side of the AP to changes in synoptic-scale circulation and the strengthening of circumpolar westerlies, mediated by a trend toward

positive polarity in the Southern Annular Mode (SAM) [*Thompson and Solomon*, 2002; *Marshall*, 2003; *Gillett et al.*, 2006], the dominant mode of atmospheric variability in the southern hemisphere [*Thompson and Wallace*, 2000]. Stronger upwind flow during positive SAM is thought to facilitate advection of air over the peninsula, leading to increases in surface temperature as the air descending over the Larsen region warms and dries. This flow pattern, observed in many parts of the world in the lee of major mountain ranges, is commonly referred to as chinook, or foehn winds. Foehn winds are characterized by dramatic and sometimes prolonged increases in lee side temperature and decreases in humidity relative to the windward side of a mountain range, with temperature changes in excess of +20°C over a time scale of hours sometimes observed as these winds replace cold air masses. Regionally, warming and drying of air as it flows over and down the leeward side of the mountain barrier can be caused by the latent heat release in the form of precipitation on the windward side of the mountain ridge, isentropic drawdown of higher altitude air toward the surface, mechanical mixing of air masses, or radiative heating of descending air [*Elvidge et al.*, 2014a, and references therein], though the exact nature of the warming is event dependent. Examining an automated weather station (AWS) record from the Larsen C, *van den Broeke* [2005] estimated that the highest modeled long-term melt rates over the Larsen B were associated with northwesterly winds, consistent with this mechanism, suggesting that higher meltwater fluxes preceded and contributed to the retreat and collapse of the ice shelf. Subsequent modeling studies have corroborated this foehn hypothesis for warming, demonstrating that strong westerly flow can lead to foehn-driven warming along the eastern peninsula [*Orr et al.*, 2008; *van Lipzig et al.*, 2008]. Other authors have observed events in situ, describing dynamics associated with specific events, quantifying their contribution to the surface energy budget and demonstrating that foehn events can cause dramatic and prolonged melt events both within and at the ice surface [*King et al.*, 2008; *Kuipers Munneke et al.*, 2012; *Elvidge*, 2013; *Scambos et al.*, 2003; *Elvidge et al.*, 2014a, 2014b; *Grosvenor et al.*, 2014]. Results from another study analyzing reanalysis datasets has also pointed to foehn winds as implicated in the regulation of coastal ice cover in the Larsen A and B embayments following ice shelf demise [*Cape et al.*, 2014].

While the dynamics as well as the surface temperature response associated with specific foehn episodes in the region of the Antarctic peninsula have therefore been relatively well described in modeling and short-term observational frameworks, long-term observations of these events have been lacking, partially owing to the remoteness and general inhospitable climate characterizing this region. Yet such long-term times series are critical, in the Antarctic and elsewhere, to ground truth the atmospheric reanalyses so commonly used in the climate literature (e.g., ERA-Interim), establish baseline climatologies, and ultimately disentangle natural and anthropogenic sources of variability in the Earth system. Trends over the Larsen A and B ice shelves have largely been examined indirectly, with long-term wind patterns for this region primarily derived from the Larsen C AWS station > 100 km south assuming similarity in regional weather patterns along the NW Weddell Sea [*van den Broeke*, 2005], and eastern AP temperature trends computed from data collected at Marambio and Esperanza stations [*Marshall et al.*, 2006], located more than 100 km north of the region of recent ice shelf collapse. Whether observations from these stations are representative of patterns observed over the former ice shelves remains uncertain.

In this study, we test the foehn hypothesis for warming of the eastern Antarctic Peninsula by analyzing a novel multidecadal surface atmospheric time series collected at the Argentine base Matienzo. In operation since 1961, the base is located on the Seal Nunataks, 30 km northwest of Robertson Island between the former Larsen A and B ice shelves and therefore situated at a critical site bordering areas of recent, rapid, and dramatic changes at the atmosphere-ice-ocean boundary. While the early part of the record has been previously analyzed [*Schwerdtfeger*, 1975, 1979], these studies focused on the dynamics of the cold, southerly barrier winds common to this region rather than the impact of foehn events on the regional climate. Using the full, high-resolution record covering two decades of observation between 1962–1975 and 1999–2010, we first describe long-term patterns in surface air temperature and test them against published trends derived from weather stations and reanalysis models. We then present the first long-term analysis of foehn winds in this region by quantifying the frequency, strength, and variability of events along the eastern AP. We relate this foehn time series to atmospheric temperatures recorded at the same site, as well as estimates of surface melt to examine the impact of foehn variability on the ice sheet and ice shelf. In so doing, we give new insight into the nature of ongoing changes along the Larsen Ice Shelf and possible future trajectories of the atmosphere-ice-ocean system, complementing previous studies of atmospheric dynamics in the region.

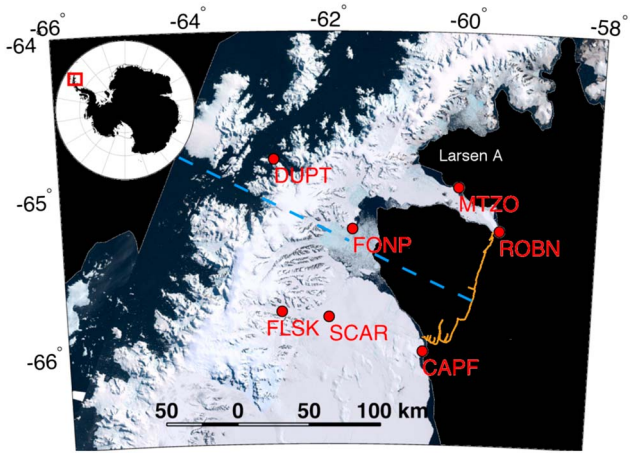

Figure 1. Map of the northern Antarctic Peninsula, showing locations of weather sensors used in this study including Duthiers Point (DUPT), Robertson Island (ROBN), Cape Frames (CAPF), Foyn Point (FONP), Flask Glacier (FLSK) SCAR Inlet (SCAR), and Matienzo (MTZO). The maximum extent of the Larsen B ice shelf in the 1960s is indicated by an orange line [*Cook and Vaughan*, 2010], while the dashed blue line represents the approximate location of the section shown in Figure 6. Further information regarding the weather stations is given in Table 1. Background image is derived from the Landsat Image Mosaic of Antarctica [*Bindschadler et al.*, 2008].

2. Data and Methods

2.1. Weather Station Records and Foehn Detection

Long-term weather records for the northern Larsen ice shelf region in the NW Weddell Sea were collected at the Argentine station Teniente Benjamin Matienzo (Figure 1 and Table 1). The base was first established in 1961, with weather data initially collected year round between 1962 and 1972, 1974–1976, and thereafter only during summer months (typically January–March) until 1987 and between 2005 and 2009 by trained military personnel of the Servicio Meteorológico Nacional under the auspices of the Argentine Air Force and later the Ministry of Defense. Temperature data were collected by precision Theodor Friedrich mercury thermometers calibrated at the Buenos Aires Regional Meteorological Instrument Center prior to deployment and each season when the base was occupied. A new suite of automated sensors installed in 1999 at the same location by members of the Instituto Antártico Argentino extended this record another decade until 2010. The data sets include measurements of temperature, relative humidity, and wind speed and direction every 3–6 h between 1962 and 1987, and every 1–3 h thereafter. Comparison of the two measurement methods using reduced major axis regression for the period of instrumental overlap between 2005 and 2009 showed a small bias, with manual measurements 0.05–0.7°C higher than AWS measurements, particularly at low temperatures (Figure S1 in the supporting information). Correcting for this bias increased the magnitude

Table 1. Weather Station Information[a]

ID	Sensor Platform	Instrument	Name	Latitude	Longitude	Elevation (m)	Earliest Data	Latest Data
DUPT	cGPS	WXT520	Duthiers Point	−64.80	−62.82	40	2009 Apr 03	2014 Aug 28
ROBN	cGPS	WXT520	Robertson Island	−65.25	−59.44	58	2010 Feb 06	2014 Aug 28
CAPF	cGPS	WXT520	Cape Framnes	−66.01	−60.56	100	2010 Feb 18	2014 Aug 28
FONP	cGPS	WXT520	Foyn Point	−65.25	−61.65	65	2010 Feb 07	2014 Aug 28
FLSK	AMIGOS	WXT520	Flask Glacier	−65.77	−62.72	450	2010 Feb 06	2014 Jul 11
SCAR	AMIGOS	WXT520	SCAR Inlet	−65.80	−62.00	54	2010 Feb 16	2014 Aug 28
MTZO	**station**	**Hg / HMP45C**	**Matienzo**	**−64.98**	**−60.07**	**25**	**1962 Jan 1**	**2010 Dec 31**

[a]ID correspond to names in Figure 1, while sensor platform distinguishes between continuously recording GPS (cGPS) stations, Automated Meteorology-Ice/Indigenous species-Geophysics Observation System (AMIGOS) sensors, and the permanent base at Matienzo (MTZO, bold). Hg corresponds to mercury thermometer, while other listings correspond to Vaisala instrument model. Note that temperature and relative humidity sensors at Matienzo were installed in a Stevenson screen. Latest data refers to date of latest data used in this analysis.

and significance of temperature trends (see below). However, due to uncertainty in the absolute error of instrumental measurements and the lack of comparable data in winter and fall months, uncorrected data were used in the rest of the analyses.

Automated weather stations installed as components of Automated Meteorology-Ice/Indigenous species-Geophysics Observation System (AMIGOS) [*Scambos et al.*, 2013] and continuously recording GPS (cGPS) [*Nield et al.*, 2014] systems further extended in situ observations around the Larsen B embayment between January 2010 and January 2013. Installed at sites surrounding and overlooking the Larsen B embayment as part of the LARISSA (LARsen Ice Shelf System, Antarctica; http://www.hamilton.edu/expeditions/larissa) project (Figure 1 and Table 1), these sensors collect data hourly and provide a spatial context for weather patterns and dynamics in this region. Meteorological data sets from the cGPS sensors were downloaded from www.unavco.org. Location of the meteorological sensors is indicated in Table 1.

Following previous studies in the Antarctic [e.g., *Speirs et al.*, 2010, 2013], we used a semi-automated selection criterion to identify the onset and cessation of foehn events from weather records. Onset was identified as an increase in temperature of 1°C h, an increase in wind speed above 5 m s^{-1} from a westerly direction, and a decrease in relative humidity of at least 5% h^{-1}. Exact wind directions for the foehn events were dependent on the location of the sensor relative to topography. For time periods when the full suite of sensor was unavailable, foehn events were primarily identified by their temperature signature. For records with lower temporal resolution (3–6 h), or during periods when only a subset of sensors were available, the criterion was adjusted and events were classified manually. All time series were manually quality controlled before analysis. Across the records, this semi-automated approach correctly classified 84% of foehn events relative to manual classification, with 8% false positives and 6% events manually added on average. The resulting time series were temporally binned by counting a day experiencing six or more hours of foehn conditions as a "foehn day." This additional criterion facilitated quantitative analysis and comparison of records. More details regarding the method can be found in *Speirs et al.* [2013] and *Steinhoff et al.* [2013].

Monthly time series of temperature and % foehn days (defined as the number of foehn days divided by number of days in the month) were generated by taking the mean and sum of daily observations, respectively. Only days and months in which 85% of observations were available were used for higher-level composites.

2.2. Atmospheric Models

Atmospheric forecast and reanalysis models were used to describe regional and synoptic-scale patterns contributing to foehn events in the Larsen B area. Archived numerical forecast output from the Antarctic Mesoscale Prediction System (AMPS) [*Powers et al.*, 2003] were downloaded from the repository at the National Center for Atmospheric Research covering the Antarctic Peninsula region (grid 6, 5 km) as well as the Antarctic continent (grid 2, 10 km) and used to describe synoptic-scale flow patterns for specific foehn events. This high-resolution model uses a polar-optimized version of the Weather Research and Forecasting (Polar WRF). AMPS incorporates the 3-dimensional variational data assimilation and the operational aspects of the Polar WRF model simulations. The Polar WRF has been shown to adequately reproduce atmospheric patterns associated with foehn events in the Antarctic, including mountain wave effects [*Steinhoff et al.*, 2014]. AMPS is initialized twice daily at 0000 and 1200 UTC. To minimize effects stemming from model initialization, only the 12–24 h forecasts from each initialization were used in this study.

The spatial and temporal characteristics of foehn events over the Larsen area are dependent on patterns of tropospheric flow upwind of the peninsula and their interaction with the mountain topography [*Elvidge et al.*, 2014b]. To estimate long-term variability in synoptic-scale flow near the Antarctic Peninsula and thereby characterize the upwind forcing of foehn events over the latter part of the Matienzo record, we obtained numerically analyzed daily atmospheric data sets from the European Center for Medium-Range Weather Forecasts ERA-Interim data set (ECMWF, http://www.ecmwf.int). Temperature and wind velocity data sets between the 1000 hPa and 800 hPa model levels at a location approximately 150 km west of Anvers Island and the Antarctic Peninsula (−63.75° latitude, −66.75° longitude, approximately one Rossby radius from the mountain range) were used to compute the nondimensional mountain height $\hat{h} = \frac{Nh}{U}$, a quantity used to characterize the response of atmospheric flow impinging upon the peninsula to deflection by the mountain range. Here N corresponds to the buoyancy frequency of the undisturbed upwind air mass, h is the height of the mountain (approximately 1400 m at the level of the Larsen B embayment), and U the mean-state layer-averaged wind speed component normal to and directed toward the AP (i.e., the U component of wind originating from 318°) [*Steinhoff et al.*, 2014]. A theoretical threshold of $\hat{h} = 1.1$ separates linear flow from

nonlinear atmospheric flow. In the case of linear flow (high velocity, weak stratification), the presence of the mountain chain represents only a weak obstacle for the incoming flow, and low-level air is easily advected over the peninsula [*Durran*, 1990]. In the case of nonlinear flow, the mountain range presents a significant barrier to atmospheric flow (e.g., for weak upwind velocities or strong stratification), potentially leading to blocking of low-level flow, mountain wave breaking, and lee side hydraulic jumps. The characteristic of the upwind flow, as described by $\hat{h}$, can have important consequences for the strength, frequency, and spatial characteristics of foehn warming over the eastern side of the peninsula. Linear flows have been shown associated with more extensive warming along the northeastern AP, with weaker temperature signatures and more topographic channeling of flow observed for nonlinear flows [*Elvidge et al.*, 2014b]. While only the single record at Matienzo is available prior to 2010, characterizing the nature of the flow over the peninsula with the more recent records as well as upwind flow characteristics gives insight into the expected spatial variability in foehn winds over the long term.

Gradients in the synoptic-scale flow field during periods of foehn winds were further examined using the daily ERA-Interim 500 hPA geopotential height data set. Standard anomaly maps of geopotential height were derived by subtracting the climatological (1979–2010) mean daily 500 hPa geopotential heights from the corresponding daily data set on a pixel-by-pixel basis and dividing by the daily climatological standard deviation. Seasonal averages of standard anomalies were then computed for days experiencing six or more hours of foehn conditions (i.e., foehn days).

2.3. Glacial Ice Melt Detection

Following the approach of *Barrand et al.* [2013] and others, we used microwave backscatter measurements from the QuikSCAT (QSCAT) Enhanced Resolution Imagery database for surface melt detection on the ice sheet and ice shelves. The data set consists of daily, enhanced resolution slice-based images spanning 1999 to 2010, derived using the Scatterometer Image Reconstruction algorithm [*Long and Hicks*, 2010], with a pixels size of 2.225 km and an effective resolution of 5 km. We defined melt on a pixel-by-pixel basis, using an austral winter mean normalized backscatter threshold approach to identify whether melt was present or absent each day and in each pixel. Daily detections were then added to yield a time series of monthly melt days covering the Antarctic Peninsula. For additional details on the method [see *Barrand et al.*, 2013, and references therein]. The QSCAT data set is available for download from the Brigham Young University NASA Scatterometer Climate Record Pathfinder (http://www.scp.byu.edu/).

2.4. Satellite Imagery

Imagery of the Antarctic Peninsula was derived from the Moderate Resolution Imaging Spectroradiometer (MODIS) on board the NASA Terra satellite. Level 1A data were obtained from the ocean color website (http://oceancolor.gsfc.nasa.gov/cms/) and processed to Level 1B using SeaDAS (http://seadas.gsfc.nasa.gov). High-resolution (500 m) true color (band 1, 645 nm; band 4, 555 nm; and band 3, 469 nm) and false color (band 3, 469 nm; band 6, 1640 nm; and band 7, 2130 nm) composite images were then generated using the SeaDAS l1mapgen processing tool.

2.5. Times Series Analyses

Standard anomaly time series were generated for in situ temperature, foehn days, and surface melt by subtracting climatological means from the monthly time series and dividing by climatological standard deviations. The correlation between two time series was then calculated using Spearman's Rank-Order Correlation, and reported as $\rho(\mathrm{d}f)$, p value, where $\mathrm{d}f = N - 2$ and N = number of pairwise cases. Least squares linear regression was used to analyze trends in the data, with results presented as b = regression coefficient when significant, $t(df) = t$ statistic, p value, where $\mathrm{d}f = N - 2$ as above. Results are presented as mean $\pm$ 95% confidence interval unless otherwise stated.

2.6. Climate Indices

We compared temperature and foehn variability to both the Southern Annular Mode (SAM) and El Niño–Southern Oscillation (ENSO), dominant modes of climate variability along the Antarctic Peninsula [*Marshall*, 2003; *Ding and Steig*, 2013]. We used the observation-based index provided by Garreth Marshall (http://www.nerc-bas.ac.uk/icd/gjma/sam.html) to characterize the state of the SAM. Positive SAM values correspond to negative atmospheric pressure anomalies at high latitudes and positive anomalies at low latitude. We used the Niño 3.4 sea surface temperature index, available at http://iridl.ldeo.columbia.edu, to characterize ENSO variability. In order to further describe seasonal and interannual variability in the synoptic-scale pressure gradient we used the Amundsen Sea Low (ASL) Relative Central Pressure Index, as well

as time series of the geographic location of the ASL, available at http://www.antarctica.ac.uk/data/absl/. The ASL is a climatological low-pressure system located in the Amundsen and Bellingshausen Seas that has been shown to significantly affect Antarctic regional and seasonal patterns of atmospheric circulation [*Hosking et al.*, 2013, and references therein], as well as foehn wind genesis near the Antarctic Peninsula [*Elvidge et al.*, 2014a].

3. Results

3.1. Interannual Temperature Variability and Trends

Seasonal and annual temperature time series and trends for the two decades of Matienzo observations are presented in Figures 2 and 3. There is a significant positive trend for mean annual temperature, with an average warming rate of 0.55 ± 0.36°C per decade (Figure 2a, $p < 0.05$), which equates to a total warming of 3.35°C from 1962–1972 to 1999–2010 (calculated as the difference in average temperature between the two decades). Statistically significant warming has occurred in every season at Matienzo, with the strongest warming occurring during winter months (June, July, August, or JJA, 0.94 ± 0.63°C per decade, $p < 0.05$, or 3.71°C average temperature difference, Figures 2 and 3). Significant positive trends (at $p < 0.05$) are also apparent for the summer (December, January, February, or DJF) and fall (March, April, May, or MAM), with rates of 0.37 ± 0.29 and 0.76 ± 0.63°C per decade (1.47 and 3.34°C total difference, respectively), while the trend during the spring months of September, October, and November (SON) is strong but only significant at the $p < 0.1$ level (0.63 ± 0.65°C per decade, 2.42°C difference). Considering only January and February months in the record, which adds seven seasons of observations to the time series between 1975 and 1985, yields similar results to the DJF time series, with an estimated rate of 0.32 ± 0.31°C per decade ($p < 0.05$,1.17°C average temperature difference between decades). The austral summer season of 2001–2002, when the last major collapse of the Larsen B ice shelf occurred, stands as the warmest season on record, with an average seasonal surface temperature of 1.3°C recorded at Matienzo [see *Skvarca et al.*, 2004].

Significant seasonal and interannual variability is, however, also evident. Annual and seasonal time series show strong 2–3 year oscillations in temperature, with mean seasonal temperatures differences between 3 and 12°C common from 1 year to the next (Figure 2). While the overall annual and seasonal trends are positive, a cooling trend is also apparent since 2004–2005 during summer and fall, indicating a potential shift in conditions since the middle of the last decade (Figures 2b and 2c).

3.2. Foehn Winds and Regional Climate

3.2.1. Case Study—25–28 March 2012

Figures 4a–4d shows the characteristic signature of a foehn wind event in the Larsen B region. This strong event, lasting from 25 to 28 March 2012, was recorded at all meteorological stations operating in the northern Larsen region up to 100 km away from the AP mountains at Robertson Island, at 450 m elevation on the Flask Glacier, as well as on board the *Nathaniel B. Palmer* 50 km offshore within the Larsen A embayment during the NBP12-03 cruise (Figure 5). Onset of the wind event was marked by a rapid increase in wind speeds to 10–15 m s^{-1} and a concurrent shift to a westerly direction. Surface temperatures around the embayment increased from an average of −10°C to +10°C and remained elevated for 12–24 h even upon relaxation of the winds, while relative humidity dropped below 50%. By comparison, the meteorological record at Duthiers Point, situated at a similar latitude at the entrance of Andvord Bay on the west side of the AP, shows only weak variability during the same period. The timing of onset and cessation of this wind event was variable across sites, with some weather stations lagging others by 2–6 h. Delay between stations may reflect the relative time taken by the winds to replace cold pools of air pushed against the eastern side of the AP mountain range or complexities arising from the nonlinear nature of mountain wave effects. Foehn clearance or decreased cloud cover over the eastern side of the AP was also apparent [*Hoinka*, 1985], with evidence of cap clouds over the ridge as well as rotor and lenticular clouds downstream from the mountain range (Figure S2) [*Durran*, 1990]. A satellite image collected by MODIS-Terra at 13:55 UTC on 26 March 2012 indicates that cloud clearance over the AP extended toward the southern reaches of the Larsen C and northward toward the tip of the Peninsula (Figure S3). Foehn cessation was marked by the rapid return of strong southerly barrier winds, as a strong low-pressure center over the Weddell Sea advected cold, continental air along the mountain range to the Larsen area, leading temperatures to drop to below −20°C and rapid sea ice formation (not shown).

The synoptic-scale atmospheric pattern associated with this surface warming is characterized by a strong meridional pressure gradient due to a low-pressure center in the southern Bellingshausen Sea driving

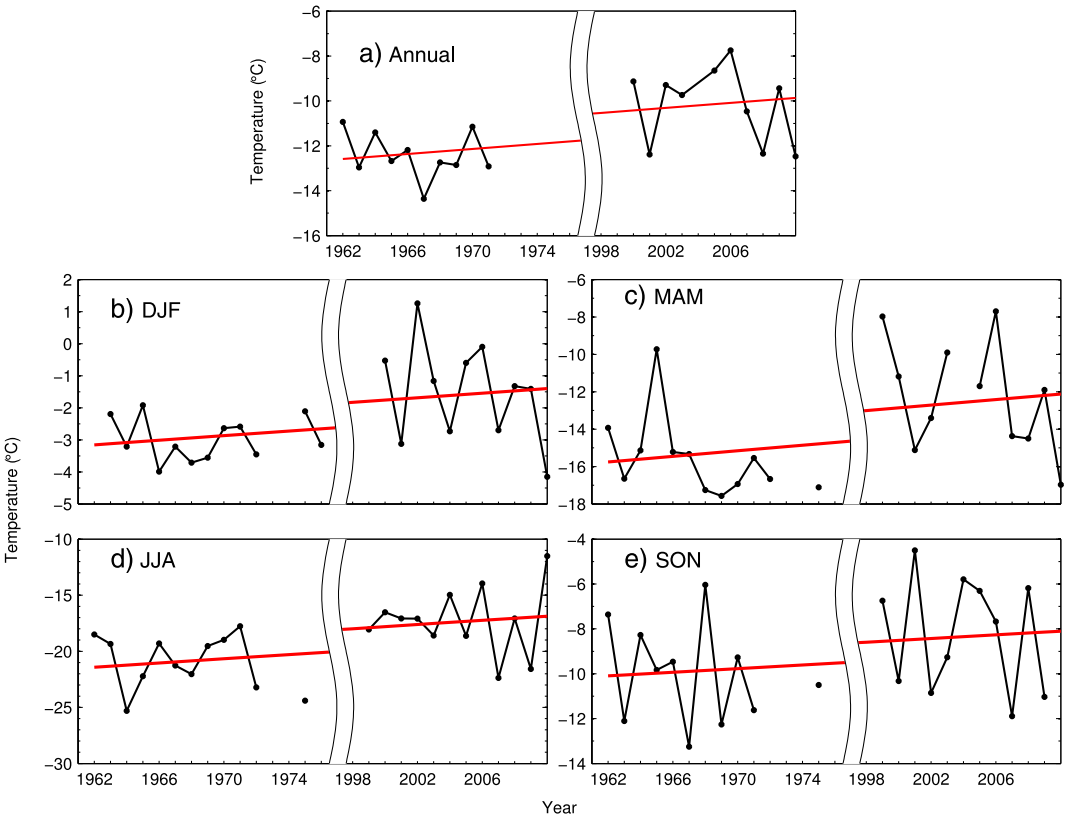

Figure 2. Mean (a) annual and (b) summer, (c) fall, (d) winter, and (e) spring temperature time series for Matienzo between 1962 and 2010. Red line denotes linear trend in the data. Note the change in temperature scale between seasons.

10–15 m s^{-1} westerly airflow impinging on the mountain range (Figures 5 and S4). The nondimensional mountain height $\hat{h}$ for this event was 1.7 for a mean upwind wind direction of 277°, indicating that nonlinear flow behavior was likely on the lee side of the mountains. During this period, the AMPS forecast for 26 March 2012, 12:00 UTC presents evidence of low-level blocking and mountain wave activity, with warm air aloft advected down toward the surface of the Larsen B embayment and elevated surface wind velocities along the lee slope and up to 100 km from the continent (Figures 6 and S5).

3.2.2. Foehn Winds as Major Features of the Eastern AP

Foehn events such the one in Figures 4–6 are commonly observed in the Matienzo record and, along with strong topographically driven southerly barrier winds [*Schwerdtfeger*, 1975; *Parish*, 1983], are distinguishing features of the wind patterns in the region. Ranging in length from several hours to occasionally weeks (Figure 7a), these events often occur in rapid succession, with extended periods showing sustained elevated surface temperatures and wind speeds. These winds demonstrate considerable seasonal variability, occurring on average between 5% and 25% of the month with maxima in the fall (SON) and minima in the summer (DJF) (Figure 7b). In extreme cases, foehn conditions can dominate monthly weather patterns with over 80% of the monthly record classified as foehn days, such as during October–December 2001, or can alternatively be completely absent (for example, December 2000 to February 2001, Figure 8). Variability in monthly foehn frequency is closely linked to the position and strength of the Amundsen Sea Low (Figure 7b). Monthly foehn frequency across both decades appeared most sensitive to the latitudinal position of the low-pressure center ($\rho(10) = -0.90, p < 0.01$, and $\rho(10) = -0.85, p < 0.01$ for 1962–1972 and 1999–2010, respectively) as well as its relative strength ($\rho(10) = -0.95, p < 0.01$, and $\rho(10) = -0.85, p < 0.01$), although strong, significant correlations were also found for longitude and absolute central pressure (not shown). Maximum foehn frequency lags both minimum central pressure and latitude by one month. The relationship between the meridional pressure gradient and foehn frequency is also apparent in the 500 hPa geopotential height anomaly field for foehn days, with negative standard anomalies in geopotential height over the Amundsen-Bellingshausen Seas varying seasonally both in magnitude and position (Figure S6). A strong center of positive geopotential height anomalies in the South Atlantic is also associated with foehn conditions over the AP across all seasons.

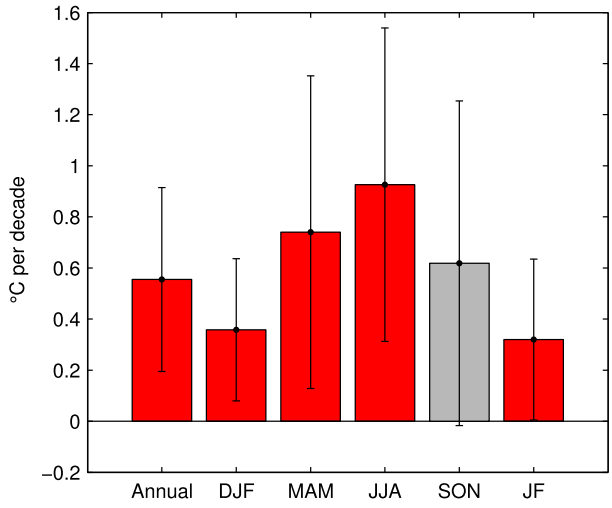

Figure 3. Summarized linear trends in annual and seasonal temperature at Matienzo between 1962 and 2010. JF denotes the January-February average, based on a longer time series than DJF. Vertical bars represent the 95% confidence intervals on the slopes. Red color denotes statistically significant trends at $p < 0.05$. Note that the SON trend is significant at the $p < 0.1$ level.

Significant interannual and interdecadal variability is observed over the two decades of observations (Figure 7c). While during 1962–1987 the record shows mainly negative anomalies in foehn days, with sporadic months of increased foehn frequency, 1999–2010 is characterized by more sustained positive anomalies, particularly early in the decade. Most notable are the years 1999, 2000, and 2001, with long periods of positive anomalies in % monthly foehn days occurring in concert with periods of major retreat in the Larsen B ice shelf. Wavelet analysis [see *Grinsted et al.*, 2004] of the foehn time series further support these observations, showing higher periodicity in the 1.5 to 4 year modes between 1999 and 2010 compared to 1962–1972, when significant variability occurred mainly at periods of 1 year or less (Figure S7).

Unlike the temperature time series, a significant positive trend in monthly % foehn days is found only in the summer (slope $= 1.46 \pm 1.26\%\,\mathrm{yr}^{-1}$, $p < 0.05$, Figure 8), with the latter decade characterized by not only higher

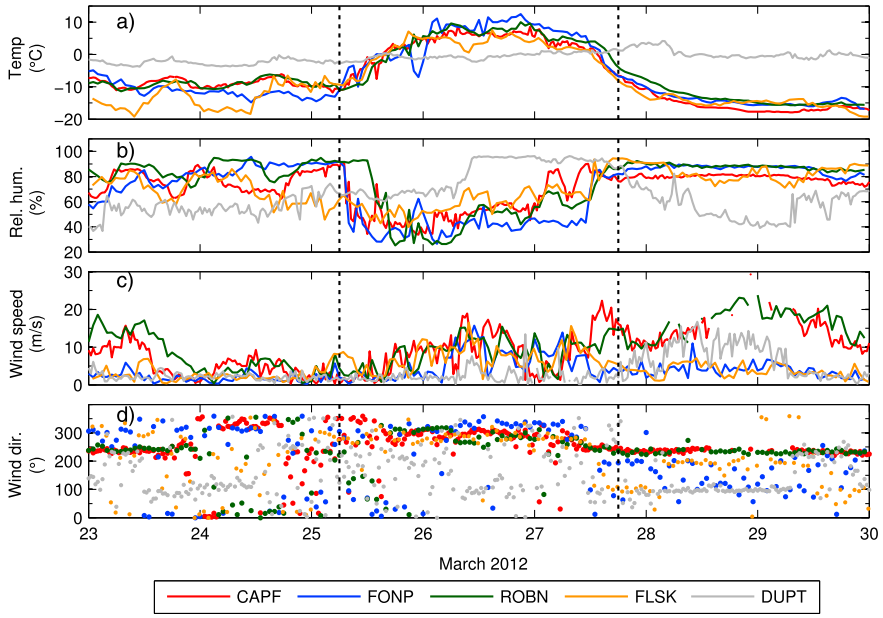

Figure 4. Meteorological characteristics of a March 2012 foehn event. Time series of (a) temperature, (b) relative humidity, (c) wind speed, and (d) wind direction for weather stations at Capes Framnes, Foyn Point, Robertson Island, and Flask Glacier along the eastern AP, and at Duthiers Point on the West Antarctic Peninsula.

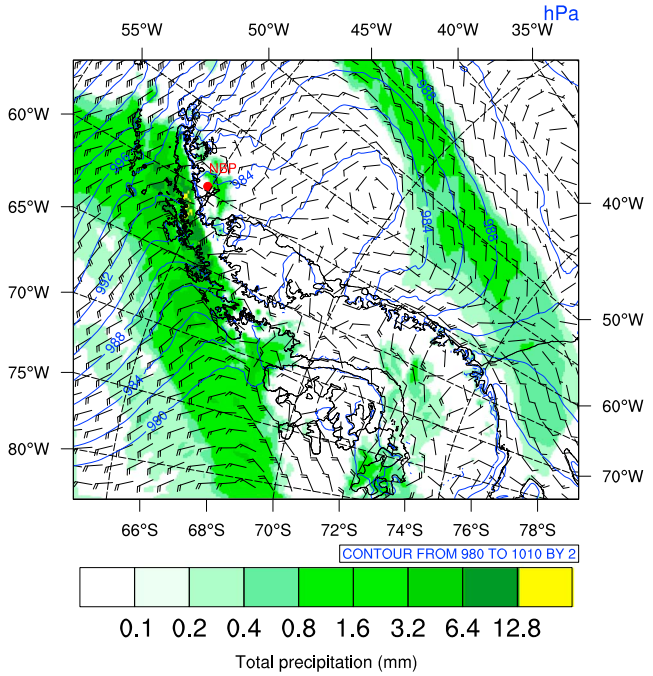

Figure 5. Antarctic Mesoscale Prediction System (AMPS) model forecast for 26 March 2012 at 12:00 UTC, showing sea level pressure (blue lines), wind vectors (black arrows), and total precipitation (green shading) during the same event. Sea level pressure is not plotted over regions exceeding 500 m elevation. The location of the RVIB *Nathaniel B. Palmer* at the start of the March 2012 foehn event is indicated by a red dot.

foehn frequency but also larger interannual variability. Although monthly foehn frequencies in October and November also appear higher during the last decade compared to 1962–1975 (Figure 7b), trends during these months and in the aggregate periods between November–February as well as October–February are not significant, though still positive ($p > 0.2$, not shown). Similarly to the temperature record (Figures 2b and 2c), a decreasing trend in foehn frequency is also present in the latter part of the decade in DJF as well as MAM (not shown).

3.2.3. Relationship Between Foehn Winds, Temperature, and Regional Climate

By advecting warm, dry air to a region that is otherwise governed by a cold, continental climate, foehn events significantly control regional climate. For the strongest foehn events in the winter and fall, surface temperature changes recorded around the Larsen embayment can exceed +30°C, with periods of above-freezing conditions lasting for days even in midwinter (Figure 7a). Characteristics of atmospheric temperature and wind during periods of foehn and nonfoehn conditions are shown for Foyn Point, a meteorological station located well within the Larsen B embayment at the base of the lee side slope (Figure 9). Analysis of observations during nonfoehn periods shows that Foyn Point is generally a low wind speed site, dominated by weak westerly winds through much of the year (Figures 9c, 9f, 9i, and 9l). Across all seasons, atmospheric temperatures during foehn events are significantly elevated relative to non foehn conditions, with temperatures on average reaching or exceeding the freezing point (Figures 9a, 9d, 9g, and 9j). As expected, winds during foehn events tend to originate from the west, with high wind speeds much more frequent relative to non foehn conditions. These general foehn characteristics hold for the entire sensor network analyzed in this study, though the various sites differ widely in the average atmospheric conditions they are exposed to. For comparison, the station at Robertson Island (ROBN) is generally characterized by much stronger southerly winds under non foehn conditions, likely an indication of the site's greater exposure to barrier winds and circulation associated with open shelf conditions (Figure S8).

Anomalies in surface air temperature and monthly foehn event frequency at Matienzo are highly correlated throughout the record ($\rho(312) = 0.62$, $p < 0.001$) and more strongly over the latter decade ($\rho(134) = 0.79$, $p < 0.001$, Figure 10a), implying a significant influence of foehn winds on regional conditions across the northern Larsen Ice Shelf area. The magnitude of surface temperature response to wind events is a function of the average seasonal temperature of surface air masses eroded by foehn winds, physical properties of the

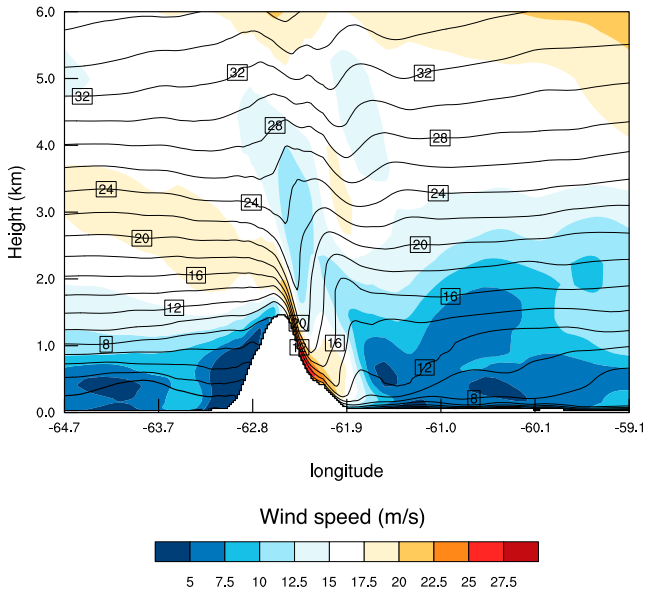

Figure 6. Vertical cross section of potential temperature (°C, black isotherms) and horizontal wind speed (m s^{-1}, color shading) along the transect shown in Figure 1 for the 26 March 2012, 12:00 UTC AMPS model forecast. White regions indicate topography, including the former Larsen B ice shelf extending between −61.9° and −59.9° longitude. Note the convergence of the < 8°C isotherms near the surface on the lee side of the peninsula, indicating warming at the lowest model levels.

surface (e.g., snow cover versus open ocean), as well as the frequency of wind events. As observed in Figure 9, the overall effect of foehn winds on average seasonal temperature is strongest during winter due to the displacement of significantly colder air masses (Figure S9), with every 1% increase in the frequency of foehn days equating to a 0.32 ± 0.15°C rise in surface air temperature ($t(22) = 4.39$, $p < 0.001$, Figure 10d). During the summer months, cyclonic activity around the peninsula is reduced due to the movement of the Amundsen Sea Low toward the peninsula (Figure S6), which leads to a northward movement of storm tracks [*Hosking et al.*, 2013] and results in a decrease in foehn frequency (Figure 6b). In turn, seasonal warming of the surface boundary layer toward the freezing point dampens the magnitude of impact of foehn winds during summer months (0.17 ± 0.05°C %$^{-1}$, $t(23) = 6.69$, $p < 0.001$; Figure S9). Rates in the fall and spring lie between these two extremes (0.24±0.17, $t(21) = 3.06$, $p < 0.01$ and 0.23±0.12°C %$^{-1}$, $t(22) = 4.07$, $p < 0.001$, respectively). Despite these seasonal differences, the remarkable lack of seasonality in monthly temperature maxima (Figure S9), all of which were recorded during westerly wind events, further underlines the powerful impact of foehn winds on eastern AP surface atmospheric variability.

3.2.4. Synoptic-Scale Drivers of Regional Variability

As observed in Figure 7, foehn events are highly variable within and between seasons, with ultimate effect on surface conditions dependent on the large-scale atmospheric flow. *Elvidge et al.* [2014a] showed that upwind tropospheric flow velocity and direction can have a major impact on the horizontal scale of the warming, with linear orographically forced response to upwind flow leading to extensive warming and high wind speeds across the entire northern Larsen C ice shelf and nonlinear response favoring more topographically constrained gap flows and a smaller horizontal footprint. While the 25–28 March 2012 event was recorded across the Larsen embayment, AMPS forecast output indicates that significant channeling of flow may have occurred (Figure S5), with near-surface high-velocity jets focusing the wind energy on the lee side of the peninsula. Observations from the NBP12-03 cruise support this prediction, with wind velocities decreasing by 20–30 m s^{-1} over the span of < 10 km during the March 2012 foehn event, despite observations of sustained high temperature and decreased relative humidity along the cruise track (not shown; see Figure 5 for ship's initial position during the event). This complex spatial response of surface conditions across the northern Larsen Ice Shelf region to foehn wind forcing is also reflected in the LARISSA weather station network. For example, whereas the March 2012 wind event was recorded at all eastern AP stations across the LARISSA network (Figure 4), others are characterized by more heterogeneous surface response, with some locations showing dramatic changes in temperature with little change in wind speed in response to the same foehn event (Figure S10).

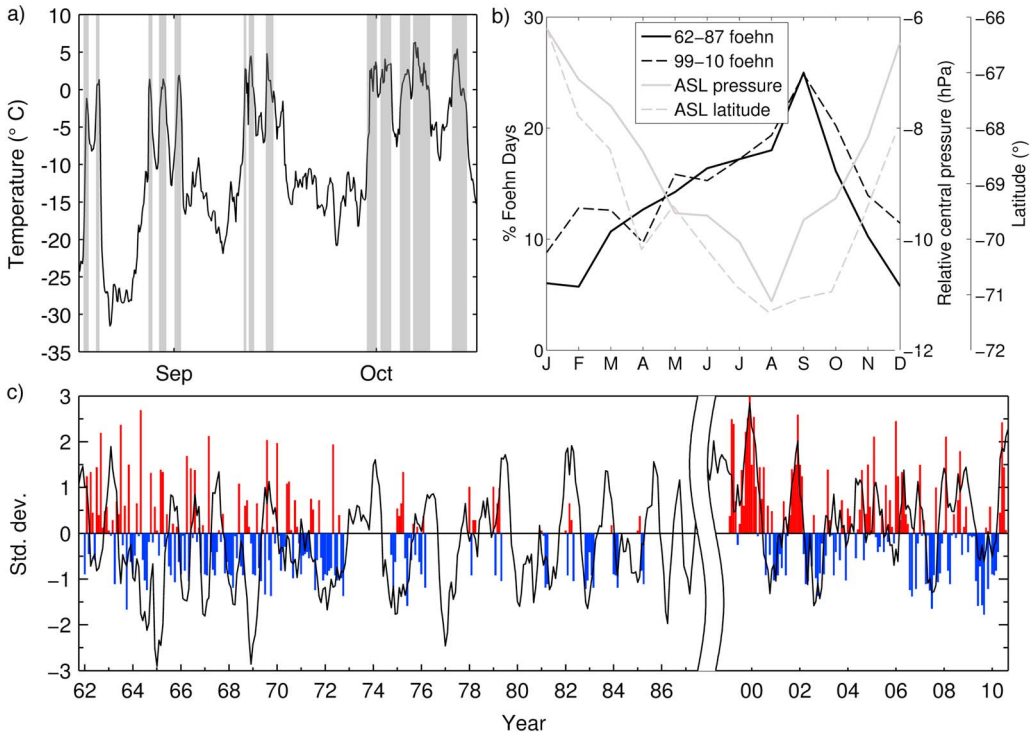

Figure 7. Temporal characteristics of foehn events. (a) Example time series of Matienzo temperature between 17 August and 15 October 2004, with shading corresponding to identified foehn events. (b) Seasonal cycle of mean monthly foehn frequency for the periods 1962–1987 (black solid) and 1999–2010 (black dashed), as well as Amundsen Sea Low relative central pressure (grey solid) and latitude (grey dashed). (c) Time series of monthly standard anomaly in foehn frequency, with positive anomalies in red and negative anomalies blue. Black line corresponds to the SAM index, smoothed using a 5 month moving average. Note the break in time series between 1987 and 1999.

We identified broad spatial and temporal foehn wind characteristics using the single record at Matienzo by exploring synoptic-scale flow variability in the ERA-Interim reanalysis data set, using foehn events identified in the observational network. Figure 11a shows a histogram of the nondimensional mountain height $\hat{h}$ for all recorded foehn events, a proxy for the expected linearity of the incoming tropospheric flow. A majority of foehn events were characterized by nonlinear upwind flow, indicating that along the NW Weddell Sea, high spatial variability in wind speeds and warming across the ice shelves and embayment are likely common, as observed in March 2012. Linear events with $\hat{h}$ <= 1.1 account for less than 10% of all observations, implying that conditions leading to an extreme spatial extent of melt over the Larsen area are uncommon. Instead, foehn flow is expected to be spatially variable, characterized by significant jets and gaps with wind speeds decreasing rapidly away from the foot of the mountains as the flow rises upward. Higher variability in $\hat{h}$ is found for northwesterly wind directions between 275° and 300° (Figure 11b). For wind directions below 275°, upwind flow tends to be linear or weakly nonlinear. Synoptic-scale atmospheric patterns show that foehn conditions tend to be associated with well-developed low-pressure systems in the Amundsen-Bellingshausen Seas and a strong meridional pressure gradient (e.g., Figures S4 and S6), with strong high pressure systems situated in the South Atlantic [see *Massom et al.*, 2006, 2008], leading to westerly advection of relatively warmer maritime air across the AP and the northern Larsen region. However, a wide array of synoptic-scale configurations appear to lead to foehn events, with slight differences in the position of weather systems having large impacts on the direction of the incoming flow, the degree of linearity, and ultimately the surface manifestation of these winds on the lee side of the peninsula.

We examined climatic links to long-term variability in temperature and foehn by considering the contribution of SAM and ENSO to synoptic-scale wind patterns and regional wind response over the northern Larsen region (Figure 7c). Overall foehn frequency shows a weak, nonsignificant upward trend between 1962 and 2010 coincident with the positive shift in the SAM over the same period [*Marshall et al.*, 2006]. Between 1962 and 1972, the foehn and SAM time series are only weakly related ($\rho(175) = 0.12$, $p = 0.19$), with few periods of synchrony between the two records. This changes for the most recent decade of 1999–2010, when the two

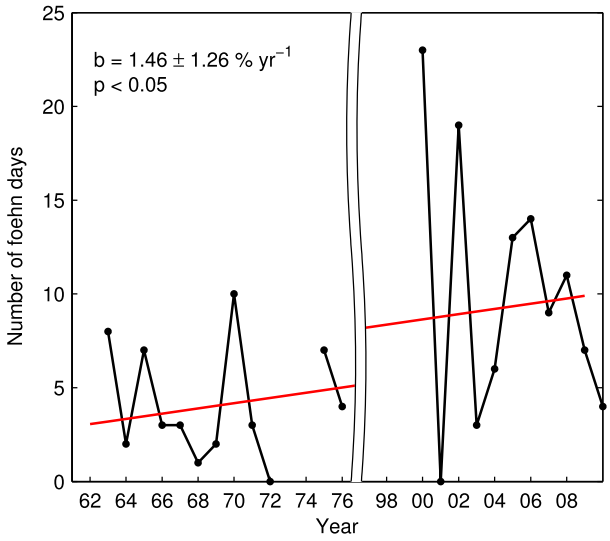

Figure 8. Foehn day time series at Matienzo between 1962 and 2010 for the summer season. Points represent sum of foehn days during DJF. Red line corresponds to linear trend.

time series are strongly correlated ($\rho(139) = 0.66, p < 0.001$). Considering seasonal averages of both time series, the SAM and foehn time series appear highly correlated over all seasons, with highest correlation in the fall ($\rho(9) = 0.91, p < 0.001$) and weakest in the summer ($\rho(9) = 0.56, p < 0.10$), while SAM and surface temperature are similarly correlated over all seasons but the summer (DJF, $\rho(9) = 0.37, p = 0.24$, Table 2). There is no significant correlation between the Niño3.4 index and the Matienzo temperature record, though a significant relationship exists with foehn days during spring ($\rho(9) = 0.55, p < 0.10$).

3.2.5. Impacts on the Cryosphere

To gain more information regarding the spatial context of this relationship and the possible contribution of foehn events to surface ice melt, we correlated anomaly time series of monthly foehn frequency and total monthly melt days for the continental ice surface derived from QuikSCAT. Over the ice sheet, significant positive correlation between wind and melt anomalies are observed prior to the collapse of the remaining ice shelf (1999–2002) and predominantly along the eastern coastline of the peninsula north of the Crane Glacier, which feeds the Larsen B embayment (Figures 12a and S11). This spatial signature, computed over a relatively short time scale, serves to highlight the impact of foehn winds both at the foot of the mountain range but also across the entire Larsen B. Although the strength of the correlation weakens when extending the time series to the full 1999–2010 time span (likely due to differences in time series length and

Table 2. Correlation of Seasonally Averaged Foehn Frequency and Temperature With Southern Annular Mode (SAM) and El Niño (Niño3.4) Indices[a]

Observation	Season	SAM	Niño3.4
Foehn Frequency (%)	DJF	0.56[b]	−0.43
	MAM	0.91[c]	−0.32
	JJA	0.58[c]	−0.48
	SON	0.71[c]	−0.55[b]
Temperature (°C)	DJF	0.37	−0.25
	MAM	0.73[c]	−0.30
	JJA	0.76[c]	−0.24
	SON	0.76[c]	−0.05

[a]Seasons are indicated by the first initial of corresponding months, i.e., DJF corresponds to the summer months of December, January, and February; MAM to March, April, May; JJA to June, July, August; and SON to September, October, November.
[b]Significance at $p < 0.1$.
[c]Significance at $p < 0.05$ or below.

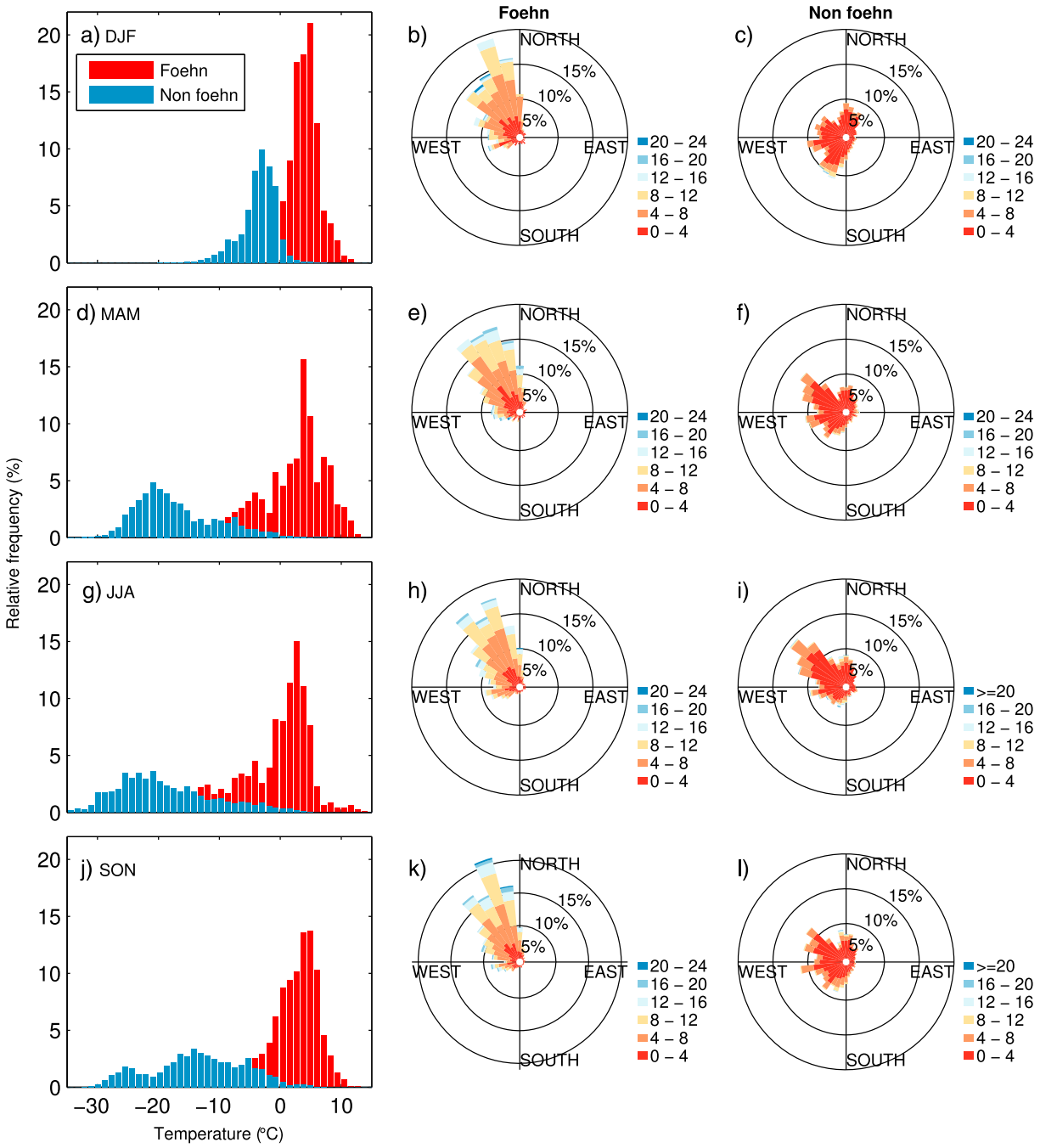

Figure 9. Characteristics of air flow at Foyn Point (FONP) for (a–c) summer (DJF), (d–f) fall (MAM), (g–i) winter (JJA), and (j–l) spring (SON). Figures 9a, 9d, 9g, and 9j show frequency histograms of temperature observations for foehn (red) and non foehn (blue) conditions, Figures 9b, 9e, 9h, and 9k wind speed and direction during foehn events, and Figures 9c, 9f, 9i, and 9l wind speed and direction during non foehn conditions. Wind speed is indicated by colors, with units of m s^{-1}. Frequency of observation is calculated relative to observations collected during foehn or non foehn periods separately (e.g., red histogram in Figure 9a shows the distribution of 100% of observations collected during foehn events in the summer months, while the blue histogram shows the distribution of 100% of the non foehn, summer observations).

variability), the spatial pattern of temporal correlations between surface melt and foehn winds remains the same (Figures 12b and S11b), with significance of the correlations increasing both along the eastern coastline and southward toward the Larsen C (Figure S11). Overall the correlation between the two time series is strongest over the Seal Nunataks, where Matienzo is located, as well as along the northern end of the Larsen A to Cape Sobral and Cape Longing ($\rho(130) = 0.55, p < 0.01$). This relationship weakens farther south over the

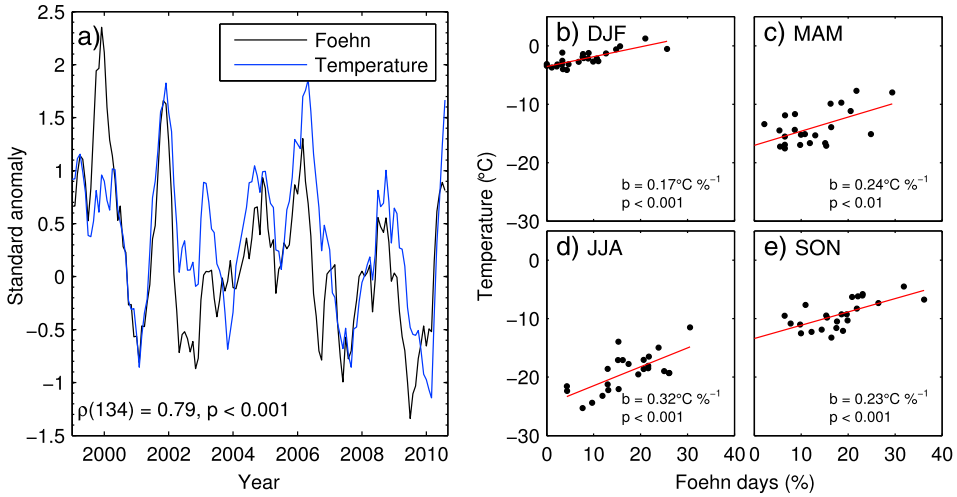

Figure 10. Relationship between foehn frequency and temperature at Matienzo. (a) Time series of standard anomalies in foehn frequency (black) and temperature (blue) between 1999 and 2010. Time series are smoothed with a 5 month moving average. Note that correlation statistics are calculated only for the period shown. Regression between mean seasonal temperature and foehn frequency at Matienzo for (b) summer, (c) fall, (d) winter, and (e) spring. Red line show linear trend in the data.

SCAR inlet, the Jason Peninsula, and the Adie and Cabinet Inlets. There is no significant correlation between the two variables over most of the Larsen C apart from narrow regions at the base of the mountain range.

The positive correlation between more frequent foehn winds and greater surface melt, as well as sustained positive SAM and positive temperature anomalies over the same period (Figure 7c), may also be reflected in the presence of an amalgamated ice layer at the surface of the ice shelf prior to its collapse (Figure 12c). As observed in an image of the outermost reach of the surface facies of the ice shelf captured near the center line position of the calving font in December 2001, the lower stratigraphy demonstrates the process of seasonal meltwater generation (superimposed ice) in tandem with winter snow to firn transitions as alternating annual bands of blue and white (respectively). This presumed normal pattern, occurring over a period of approximately 20 years as inferred by the annual banding, is abruptly terminated by a

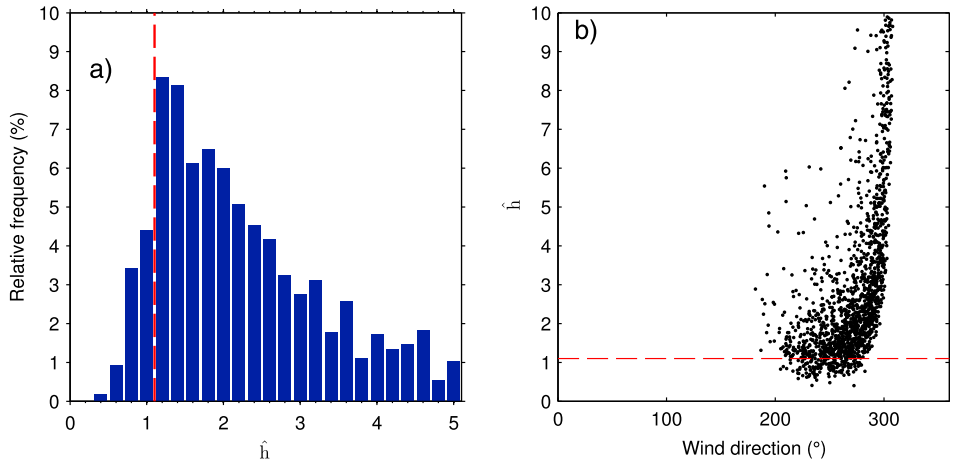

Figure 11. Atmospheric flow characteristics estimated from ERA-Interim reanalysis field. (a) Histogram of nondimensional mountain height, $\hat{h}$, for all foehn events between 1999 and 2010 computed at a location 150 km west of the Antarctic Peninsula (−63.75° latitude, −66.75° longitude). Only $\hat{h}$ values below 5 are shown (80% of all occurrences). (b) Scatterplot of wind direction averaged between the 1000 and 800 hPa ECMWF model levels (approximately 200–1000 m) versus nondimensional mountain height for foehn events, calculated at the same point as Figure 11a. Red vertical (Figure 11a) and horizontal (Figure 11b) lines correspond to the theoretical threshold of $\hat{h} = 1.1$ separating linear (lower values) from nonlinear flow (> 1.1).

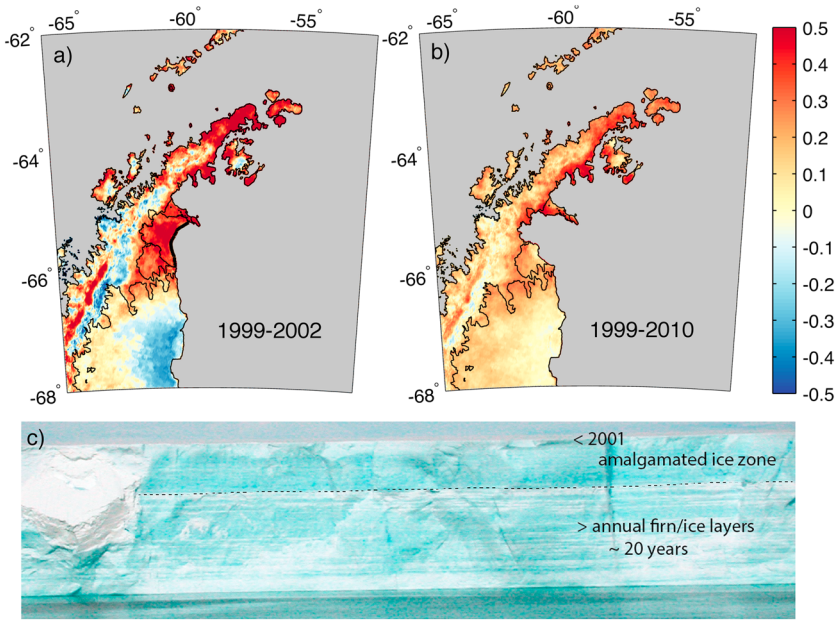

Figure 12. Spatial pattern of temporal correlation between the monthly foehn anomaly time series and total monthly backscatter-derived melt days over the ice sheet for (a) 1999–2002, with ice shelf extent indicated by the thick black line and (b) 1999–2010. Significance of correlation (*p* value) is shown in Figure S11. The coastline is derived from the Mosaic of Antarctica [*Scambos et al.*, 2007]. Correlations over the former Larsen B ice shelf were masked in Figure 12b due to its collapse after 2002. (c) Cross section of the Larsen B ice shelf captured along its centerline in December 2001 prior to its collapse. The horizontal dashed line separates a lower zone of seasonally alternating firn/ice layers from an upper zone of amalgamated ice indicative of greater seasonal melt, percolation, and refreezing in the years leading up to the breakup.

superimposed ice layer approximately 2–4 m thick near the surface, consistent with enhanced melt, percolation, and refreezing of all of the winter snow-firn in the years leading up to the 2001 collapse.

4. Discussion

Understanding the physical mechanisms underlying increasing temperature trends and their impacts on the cryosphere at both poles is critical to forecasting changes in these regions and deducing their implications for the Earth system. While contemporary studies have emphasized the consequences of a warming ocean and enhanced ice-ocean interactions for ice sheet thinning and retreat, including recently over the Larsen C [*Jacobs et al.*, 2011; *Pritchard et al.*, 2012; *Rignot et al.*, 2014; *Holland et al.*, 2015], several Antarctic ice sheet catchments are fronted by ice shelves that have significant present-day melt rates but relatively little intrusion of warm deep water [*Liu et al.*, 2006; *Tedesco*, 2009]. The retreat and collapse of the Larsen A and B ice shelves in the last three decades demonstrated the power of gradual changes in air temperature and atmospheric circulation on ice sheet dynamics, quickly becoming a compelling example of the impact of climate change on polar regions [*Scambos et al.*, 2003; *van den Broeke*, 2005; *Domack et al.*, 2005]. The weather record from Base Matienzo collected over two decades provides valuable evidence of the rapid increases in temperature experienced in this region, while also giving the first observational account of the link between long-term variability in synoptic-scale circulation (e.g., SAM), foehn winds, and temperature over the northern Larsen Ice Shelf region. This relationship manifests itself both in the significant trends observed in both SAM and surface temperature, as well as the significant correlation between the SAM index, surface temperature, and the derived foehn frequency time series.

4.1. Matienzo Temperature Trends in Context

The Matienzo record confirms that the Larsen A and B region of the eastern AP has experienced a sustained and significant increase in atmospheric temperatures, with warming evident in all seasons and on an annual basis. The rates of warming derived in this study, ranging from +0.37 to +0.94°C per decade (Figure 3), are far higher than the global average and are some of the highest measured across the Antarctic continent [*Bromwich et al.*, 2013], although caution must be exercised in interpreting these rates due to the significant gap in the Matienzo time series. Temperature trends are also in agreement with those recently derived

for the Antarctic Peninsula and West Antarctica in a new reconstruction of Antarctic near-surface temperatures [*Nicolas and Bromwich*, 2014], which highlights both the widespread nature of these temperature changes across the continent and the magnitude of changes along the eastern AP. These warming rates are also comparable to those previously published for the Argentine Station Marambio farther north near the tip of the peninsula, which has frequently been used as the reference station for the eastern AP [e.g., *Marshall et al.*, 2006]. Yet only summer and annual trends were found to be significant in the Marambio record with spring showing no trend, while trends at Matienzo are positive and significant across all seasons as well as annually (Figure 3). This notable discrepancy underscores the need for careful extrapolation when considering spatial trends in observationally limited regions.

Linking upper level atmospheric flow to the west to surface conditions on the east side of the Antarctic Peninsula, foehn winds induce dramatic positive surface temperature anomalies over time scales of hours to days that ultimately affect seasonal temperature and long-term atmospheric trends (Figures 4, 5, 7a, 9, and 10). The influence of these winds on surface weather has already been highlighted in both modeling [*Orr et al.*, 2008; *van Lipzig et al.*, 2008], as well as observational studies for specific events recorded farther south over the Larsen C [*Elvidge*, 2013; *Kuipers Munneke et al.*, 2012; *Elvidge et al.*, 2014a]. Similar observations have been made using AWS for foehn events in the McMurdo Dry Valleys, where foehn winds are responsible for a majority of positive degree days [*Speirs et al.*, 2013; *Steinhoff et al.*, 2014]. Over the northern Larsen region, periods of positive temperature, conducive to higher melt rates, are almost exclusively associated with periods of westerly downslope winds (Figure 9), with negligible contribution from northeasterly winds as previously posited by *van den Broeke* [2005]. Although on average occurring only during a maximum of 25% of the month (Figure 7b), foehn wind frequency explains over 60% of the variability in monthly surface temperatures between 1962 and 2010 (Figure 10a), with higher average seasonal temperatures associated with increases in foehn frequency (Figures 10b–10d). Their impact is particularly pronounced seasonally between March and October when otherwise cold, continental conditions can be rapidly interrupted by temperature excursions above the freezing point (Figures 7a, 9, and S9).

4.2. Scales of Atmospheric Variability

Variability in the spatial and temporal characteristics of foehn winds is linked to interacting processes occurring on multiple scales, ranging from the strength and path of individual storm tracks around the Antarctic Peninsula, seasonal changes in synoptic-scale circulation (e.g., position and strength of the Amundsen Sea Low, Figure 7b), to synoptic-scale climate variability (i.e., SAM, Figure 7c and Table 2). Previous studies have shown that the movement of cyclones around the Antarctic Peninsula can influence the surface signature of foehn events due to slight changes in both wind direction and vertical source of the air mass advected over the peninsula, affecting both the amplitude of temperature change and the spatial distribution of warming over the Larsen C [*Elvidge et al.*, 2014b]. Nonlinear flow over the peninsula, dominant during foehn events in this region (Figure 11), results in higher-amplitude warming primarily in the immediate lee of the mountain range, while linear flow is associated with extensive warming across the entire region. This variability is captured across our sensor network in the often heterogenous response of surface conditions to upwind flow (Figures 4 and S10), which serves to highlight the importance of placement of automated weather stations in the study of such phenomena [*Grosvenor et al.*, 2014]. In the case of the Larsen C, aircraft and modeling observations also identified mesoscale foehn jets, resulting from the flow of air through gaps in the AP topography, channeling higher-level flow toward the surface of the ice shelf, with adjacent wake regions characterized by weaker winds but higher temperatures [*Elvidge et al.*, 2014a, 2014b]. Similar features were observed over the Larsen A and B for a 2012 foehn event, both in situ and in atmospheric forecasts (Figures 4 and S5). While this study focused primarily on the relationship between large-scale and long-term atmospheric variability, foehn dynamics, and temperature trends over the Larsen region, the foehn time series could be used to analyze in greater detail the dynamics associated with the interaction of synoptic-scale flow with the Antarctic Peninsula, which could in turn lead to improvements in atmospheric forecasts and greater insight into the long-term changes in the region.

Over seasonal timescales, foehn wind frequency along the AP appears closely linked to changes in the meridional pressure gradient, and particularly the seasonal variability in the position and strength of the Amundsen Sea Low (Figure 7b). Summer periods, at which time the ASL is generally weaker and located farther east and north, are associated with lower foehn frequency, while winter and spring periods are associated with higher foehn frequency due to the stronger meridional gradient induced by the westward and poleward movement and deepening of the ASL (Figure 7b). Its position and strength in turn influence the trajectories of cyclones

and airflow across the Antarctic Peninsula, likely causing variability in the surface expression of foehn events over the Larsen region. This relationship between ASL characteristics, foehn winds, and ultimately temperature is in agreement with previous studies, which highlighted the importance of the ASL for West Antarctic climate [*Hosking et al.*, 2013].

While the dynamics of the ASL appears to determine seasonal variability in foehn events over the Larsen Ice Shelves, lower latitude processes also likely play an important role in controlling atmospheric flow around the peninsula. For example, the presence of a strong blocking high-pressure system in the South Atlantic during the austral summer seasons 2001–2002 and 2004–2005 was associated with extreme anomalous atmospheric circulation across the Antarctic Peninsula [*Massom et al.*, 2006, 2008], with repercussions on sea ice extent, surface temperatures, and as demonstrated in this study foehn wind frequency along the eastern AP (Figure 7c). Considering the decade of observation between 1999 and 2010, episodes of strong positive anomalies in both temperature and downslope wind events at Matienzo were also associated with enhanced meridional gradients, with negative 500 hPa geopotential height anomalies over the Amundsen-Bellingshausen region coincident with positive anomalies over the South Atlantic (Figure S6), implying a link between subtropical circulation and Antarctic Peninsula climate. The position and strength of the South Atlantic anticyclone, a semipermanent synoptic-scale system, may therefore also contribute to wind variability along and across the AP and may explain some of the anomalies observed in regional circulation patterns [*Lübbecke et al.*, 2014]. The nature of this connection will be investigated in a follow-up study. While affecting windward atmospheric patterns, strong cross-peninsula flow can also have a significant impact on atmospheric circulation over the Weddell Sea, with cyclogenesis in the lee of the AP further reinforcing the dominant southerly flow, as observed in March 2012 (Figures 4 and S4) [*Turner et al.*, 1998; *Lubin et al.*, 2008; *King and Turner*, 2009]. The effect of westerly flow on mean surface temperature and foehn frequency is therefore complex, involving atmospheric dynamics on both sides of the AP as well as interactions between low and high latitudes.

Shifts in the Southern Annular Mode have been frequently cited as the root cause of temperature increase along the AP [*Marshall et al.*, 2006; *Orr et al.*, 2008] and were found in this study to be significantly positively correlated with both temperature and foehn frequency along the eastern AP (Figure 7c and Table 2). This strong relationship holds over all seasons but the summer (DJF), for which comparatively weaker correlations between temperature and SAM are found (Table 2). By comparison, a significant relationship between ENSO and foehn winds was only present for the spring (SON), indicating a limited influence of tropical variability on eastern AP temperature variability. However, recent studies have highlighted the influence of tropical and ENSO variability on the SAM itself [*Ding and Steig*, 2013; *Ding et al.*, 2014], implying a complex relationship between these modes of climate variability [*Turner*, 2004]. The large synchronous excursions of wind forcing, temperature, and SAM are particularly noteworthy between 1999 and 2002, a period characterized by extensive surface melt, retreat, and collapse of the Larsen B ice shelf (Figures 2 and 7c) [*Scambos et al.*, 2000]. These results further support the aforementioned link between climate variability, synoptic-scale circulation, and downslope wind response in the Larsen area (Figure 7) and more broadly the foehn hypothesis for warming of the eastern AP [*van den Broeke*, 2005; *Marshall et al.*, 2006]. While the impact of individual foehn events on temperature is generally ephemeral due to their localized nature, periods of foehn winds tend to be characterized by a rapid succession of events over days to weeks (e.g., Figure 7a), leading to prolonged periods of temperature anomalies that in aggregate significantly increase average surface temperature [*Steinhoff et al.*, 2014]. Physically, the rapid succession of foehn events could prevent the formation of a strong surface inversion layer or the pooling of cold air against the peninsula mountain range, thereby enhancing the impact of subsequent foehn events on surface conditions. The amplitude of foehn events, posited along with foehn frequency as underlying the positive temperature trend, comparatively showed no significant trend or relationship with climate indices (not shown). Although foehn amplitude may have a tremendous impact on the warming signal of individual events, frequency of downslope wind events therefore appears primarily responsible for the observed surface temperature variability over the latter part of the twentieth century.

Significant trends in the SAM have been identified over summer and fall, as well as on an annual timescale [*Marshall*, 2003; *Marshall et al.*, 2006]. While these increases are reflected in the significant trend in foehn frequency during summer (Figure 8), positive trends during other seasons were weak and nonsignificant. Yet correlations between SAM and foehn frequency are significant across all seasons, and particularly strong during the fall (Table 2). Further examination of temperature and wind data sets reveals a distinct increase between 1962–1972 and the 1999–2002 period, in agreement with concomitant trends in the SAM, followed

annually and in all seasons but the winter by a rapid decrease (Figures 2 and 8). This apparent cooling trend, paralleled by foehn frequency decreases, is further corroborated by a regional temperature history derived from isotope analysis of an ice core collected on the Bruce Plateau overlooking the Larsen B embayment [*Zagorodnov et al.*, 2011], which shows a maximum in temperature between 1995 and the early 2000s followed by a rapid decrease. These observations may indicate a return to more dominant cold, continental conditions characteristics of the early decade, and a switch in synoptic-scale forcing impacting regional wind patterns. Although the high variability in foehn frequency, and the lack of data between 1987 and 1999, precludes further analysis of trends during this critical period, reconstructions of surface temperatures using atmospheric reanalysis models linked to surface observations may shed light on the evolution of atmospheric forcing during this missing decade.

4.3. Implications for Surface Melt

The strong correlation between downslope winds and monthly satellite-derived melt estimates, although only a first-order approximation due to the other potential sources of inherent variability in melt patterns (e.g., elevation, variability in nonfoehn atmospheric circulation), support the notion that foehn winds significantly impact landscape processes, including glacial melt, both along the eastern AP and elsewhere. *van den Broeke* [2005] initially showed high melt rates associated with northeasterly and northwesterly winds preceding the Larsen B collapse, hypothesizing that foehn winds contributed to ice shelf demise. The Matienzo record further confirms that westerly winds contributed significantly to surface warming, while showing negligible contribution from northeasterly winds (Figure 9). In the Dry Valleys, downslope winds are thought to play a major role in controlling glacial melt rates and streamflow variability [*Doran et al.*, 2008; *McGowan et al.*, 2014], with variability over geological timescales affecting the regional climate and contributing to waxing and waning of large valley-floor lakes [*Hall et al.*, 2001; *McGowan et al.*, 2014]. In the same region, the impacts of discrete periods of sustained foehn winds (weeks-month) on both physical landscape (melt, stream flow, and soil temperature) have also been shown to far outlive the length of the events themselves, with lasting impacts on the ecosystem [*Barrett et al.*, 2008]. Over the Larsen C, *Elvidge* [2013] showed using modeling that large downward solar radiation due to clear-sky conditions (e.g., Figures S2 and S3) and sensible heat fluxes from air to ice are responsible for warming of the ice surface, with the highest rates of melt induced by strong, linear foehn events. More recently, results from *Grosvenor et al.* [2014] showed that shortwave input dominated the melting signal, further evidence of the importance of variability in cloud cover for surface energy balance. Heat flux calculations computed by *Kuipers Munneke et al.* [2012] for a particular event found $> 100\,\mathrm{W\,m^{-2}}$ of residual energy available for melting. These previous results demonstrate the extensive impact of these winds on the ice sheet, and the potential for feedbacks between foehn events and surface melt due to their effects on surface albedo as well as radiative fluxes.

Gradients in the foehn-melt correlation demonstrate that the Larsen region, particularly at the base of the mountain range and within the numerous inlets and glaciers, are most sensitive to wind-driven melting (Figures 12 and S11). Notably, a strong relationship is apparent over the Larsen B ice shelf prior to its collapse in between 1999 and 2002, and otherwise coastal regions adjoining the Larsen A and B embayments, the remnant SCAR Inlet, as well as the inlets along the northern Larsen C. Enhanced surface melting and melt ponds in the immediate lee of the mountain range, cited as the signature of foehn-induced melt, have been commonly reported over the eastern peninsula in studies of optical, backscatter, and passive microwave imagery [*Scambos et al.*, 2004; *Barrand et al.*, 2013; *Trusel et al.*, 2013; *Luckman et al.*, 2014], with patterns further reproduced in modeling studies [*Elvidge et al.*, 2014b; *Grosvenor et al.*, 2014]. Weaker correlations over the Larsen C south of Cape Framnes in the present data set may indicate either comparatively reduced foehn activity in the region, fundamental changes in foehn dynamics due to differing mountain orography, or differences in the climatological setting of the region. Regardless, these melt observations are also qualitatively similar to ice sheet densification patterns observed over the Larsen B and northern Larsen C [*Holland et al.*, 2011], a process resulting from repeated surface melt and percolation leading to decreases in air content, which is thought to have contributed to the destabilization of the ice shelf. The densification process was recently observed over the remnant Larsen B during a foehn event, with firn temperature measurements collected by the SCAR Inlet AMIGOS showing significant surface warming outliving the end of the wind event and percolation of melt to 1 m depth [*Scambos et al.*, 2013], along with extensive ablation of the surface snow cover due to melt, evaporation, and sublimation. The densification hypothesis is also supported by the transition between regular annual bands of snow-firn and ice and a near-surface region of amalgamated ice observed in the frontal ice shelf stratigraphy prior to the collapse (Figure 12c). This sharp transition

likely corresponds to a period in the late 1980s and mid-1990s during which Landsat imagery indicates rapid spreading of melt ponds from the Hektoria grounding line region across the ice shelf to the ice front as well as extended periods of melt across the region [*Scambos et al.*, 2003]. While Figure 12c presents evidence in support of the foehn-melt mechanism of ice shelf collapse, care must be taken in interpreting such images given the complexity of firn processes and melt migration [e.g., *Das and Alley*, 2008], and the lack of independent chronology for the observed ice shelf stratigraphy. The numerous lines of evidence nevertheless underscore the fundamental role played by foehn winds in controlling glacial melt processes along the AP.

5. Conclusions

In aggregate, the weather observations collected at Matienzo present a strong case for the role of foehn winds in the collapse of the Larsen B ice shelf via their impact on surface climate, and ultimately glacial melt rates. Key to these conclusions are the parallels between periods of sustained positive SAM and foehn wind forcing (Figures 7c and 8), temperature increases (Figures 2 and 10), and surface melt (Figure 12) preceding ice shelf retreat and collapse events in 2000 and 2002. Unlike over the Larsen C, the fingerprint of foehn events on surface melt is apparent over the entire Larsen B ice shelf prior to its collapse (Figure 12a). With melt evident up to 100 km from the coast, these observations are consistent with the spatial extent of foehn warming observed by the LARISSA AWS network (Figure 4) and a testament to the westerly winds' fundamental impact on surface conditions. While in broad agreement with previous findings derived from more distant weather stations [e.g., *van den Broeke*, 2005; *Marshall et al.*, 2006], discrepancies in the significance and magnitude of temperature trends as well in observed circulation patterns in the Larsen A/B region highlight the potential errors arising from spatial extrapolation. Observations of structural ice shelf characteristics using satellite imagery have indicated that the time span between 1962 and 1986 corresponded to a period during which the Larsen B ice shelf was likely in steady state [*Skvarca et al.*, 1999b]. Weather records during this period are likewise relatively consistent, with little to no trend in either foehn or temperature (Figures 2 and 8). Conversely, increased shear zone stress and fracturing was evident on the ice shelf surface between 1986 and 1998, implying a rapid change in conditions during that time. The dramatic collapse in 2002 was then the concluding chapter of a long chain of events leading to the gradual breakdown of the structural integrity of the ice shelf. While the trends in the Matienzo record show evidence of increases in both foehn winds and temperature corresponding with this evolving ice shelf geometry, this critical period is missing from the weather record due to constraints on budgets, equipment, and manpower. Integration of this time series into high-resolution atmospheric models could, however, be used to reconstruct the surface temperature record during this period [e.g., *Bromwich et al.*, 2013], yielding further insight into the relationship between atmospheric processes and ice sheet mass balance. Additionally, sustained instrumentation of regions of imminent ice shelf collapse, such as the SCAR Inlet Ice Shelf [*Scambos et al.*, 2013], would provide invaluable insight into the dynamics linking atmospheric variability, meltwater production and percolation, and ice shelf integrity. Given the widespread thinning and retreat of ice shelves across the Antarctic Peninsula and the continent as a whole [*Pritchard et al.*, 2012; *Cook and Vaughan*, 2010; *Paolo et al.*, 2015], continued observations linked to high-resolution models could in turn shed light on the potential future of other ice shelves in regions of rapid warming.

Acknowledgments
The authors acknowledge Argentine scientists, staff, and members of the Servicio Meteorológico Nacional, Argentina, responsible for the establishment and maintenance of the weather station at Matienzo; Matthew Lazarra and the staff of the Antarctic Meteorological Research Center at the University of Wisconsin, Madison, for assistance with automated weather station data processing; the captain and crew of RVIB *Nathaniel. B Palmer* and R/V *Laurence M. Gould*; Raytheon Polar Services technicians; and PHI, Inc. helicopter pilots and mechanics for assistance with instrument deployment during LMG0903, NBP1001, and NBP1203. Discussions with Lihini Aluwihare, Peter Franks, Jonathan Shurin, and Sarah Gille significantly improved the manuscript. Kevin Manning provided valuable input for the analysis of AMPS forecasts, while Johanna Speirs and Andrew Elvidge gave helpful advice for the analysis of foehn wind events. Gabe Kooperman provided assistance with interpretation of AMPS output. We would like to acknowledge high-performance computing support from Yellowstone (ark:/85065/d7wd3xhc) provided by NCAR's Computational and Information Systems Laboratory, sponsored by the National Science Foundation. The authors also thank three anonymous reviewers, whose comments and suggestions significantly improved the manuscript. This work was supported by the National Science Foundation Office of Polar Programs under NSF grants ANT-0732983, ANT-0732467, and ANT-0732921. M.R.C. was also supported by the NSF Graduate Research Fellowship under grant DGE-1144086 and by NASA Headquarters under the NASA Earth and Space Science Fellowship Program—grant NNX12AN48H. The data are available as indicated in the methods section and otherwise from the authors upon request (mcape@whoi.edu).

References

Abram, N. J., R. Mulvaney, E. W. Wolff, J. Triest, S. Kipfstuhl, L. D. Trusel, F. Vimeux, L. Fleet, and C. Arrowsmith (2013), Acceleration of snow melt in an Antarctic Peninsula ice core during the twentieth century, *Nat. Geosci.*, *6*(5), 404–411, doi:10.1038/ngeo1787.

Barrand, N. E., D. G. Vaughan, N. Steiner, M. Tedesco, P. Kuipers Munneke, M. R. van den Broeke, and J. S. Hosking (2013), Trends in Antarctic Peninsula surface melting conditions from observations and regional climate modeling, *J. Geophys. Res. Earth Surf.*, *118*, 315–330, doi:10.1029/2012JF002559.

Barrett, J. E., R. A. Virginia, D. H. Wall, P. T. Doran, A. G. Fountain, K. A. Welch, and W. B. Lyons (2008), Persistent effects of a discrete warming event on a polar desert ecosystem, *Global Change Biol.*, *14*(10), 2249–2261, doi:10.1111/j.1365-2486.2008.01641.x.

Bindschadler, R., P. Vornberger, A. Fleming, A. Fox, J. Mullins, D. Binnie, S. J. Paulsen, B. Granneman, and D. Gorodetzky (2008), The Landsat image mosaic of Antarctica, *Remote Sens. Environ.*, *112*(12), 4214–4226.

Bromwich, D. H., J. P. Nicolas, A. J. Monaghan, M. A. Lazzara, L. M. Keller, G. A. Weidner, and A. B. Wilson (2013), Central West Antarctica among the most rapidly warming regions on Earth, *Nat. Geosci.*, *6*(2), 139–145, doi:10.1038/NGEO1671.

Cape, M. R., M. Vernet, M. Kahru, and G. Spreen (2014), Polynya dynamics drive primary production in the Larsen A and B embayments following ice shelf collapse, *J. Geophys. Res. Oceans*, *119*, 572–594, doi:10.1002/2013JC009441.

Cook, A. J., and D. G. Vaughan (2010), Overview of areal changes of the ice shelves on the Antarctic Peninsula over the past 50 years, *Cryosphere*, *4*(1), 77–98, doi:10.5194/tc-4-77-2010.

Das, S. B., and R. B. Alley (2008), Rise in frequency of surface melting at Siple Dome through the Holocene: Evidence for increasing marine influence on the climate of West Antarctica, *J. Geophys. Res.*, *113*, D02112, doi:10.1029/2007JD008790.

Ding, H., R. J. Greatbatch, and G. Gollan (2014), Tropical influence independent of ENSO on the austral summer Southern Annular Mode, *Geophys. Res. Lett.*, *41*, 3643–3648, doi:10.1002/2014GL059987.
Ding, Q., and E. J. Steig (2013), Temperature change on the Antarctic Peninsula linked to the Tropical Pacific, *J. Clim.*, *26*(19), 7570–7585, doi:10.1175/JCLI-D-12-00729.1.
Domack, E., D. Duran, A. Leventer, S. Ishman, S. Doane, S. McCallum, D. Amblas, J. Ring, R. Gilbert, and M. Prentice (2005), Stability of the Larsen B ice shelf on the Antarctic Peninsula during the Holocene epoch, *Nature*, *436*(7051), 681–685, doi:10.1038/nature03908.
Doran, P. T., C. P. McKay, A. G. Fountain, T. Nylen, D. M. McKnight, C. Jaros, and J. E. Barrett (2008), Hydrologic response to extreme warm and cold summers in the McMurdo Dry Valleys, East Antarctica, *Antarct. Sci.*, *20*(5), 499–509, doi:10.1017/S0954102008001272.
Durran, D. R. (1990), Mountain waves and downslope winds, *Meteorol. Monogr.*, *23*(45), 59–83.
Elvidge, A. D. (2013), Polar föhn winds and warming over the Larsen C Ice Shelf, Antarctica, PhD thesis, Univ. of East Anglia, Norwich, U. K.
Elvidge, A. D., I. A. Renfrew, J. C. King, A. Orr, T. A. Lachlan-Cope, M. Weeks, and S. L. Gray (2014a), Foehn jets over the Larsen C Ice Shelf, Antarctica, *Q. J. R. Meteorol. Soc.*, *141*, 698–713, doi:10.1002/qj.2382.
Elvidge, A. D., I. A. Renfrew, J. C. King, A. Orr, and T. A. Lachlan-Cope (2014b), Foehn warming distributions in nonlinear and linear flow regimes: A focus on the Antarctic Peninsula, *Q. J. R. Meteorol. Soc.*, doi:10.1002/qj.2489.
Gillett, N. P., T. D. Kell, and P. D. Jones (2006), Regional climate impacts of the Southern Annular Mode, *Geophys. Res. Lett.*, *33*, L23704, doi:10.1029/2006GL027721.
Grinsted, A., J. C. Moore, and S. Jevrejeva (2004), Application of the cross wavelet transform and wavelet coherence to geophysical time series, *Nonlinear Processes Geophys.*, *11*(5–6), 561–566, doi:10.5194/npg-11-561-2004.
Grosvenor, D. P., J. C. King, T. W. Choularton, and T. Lachlan-Cope (2014), Downslope föhn winds over the Antarctic Peninsula and their effect on the Larsen ice shelves, *Atmos. Chem. Phys.*, *14*(18), 9481–9509, doi:10.5194/acp-14-9481-2014.
Gutt, J., et al. (2011), Biodiversity change after climate-induced ice-shelf collapse in the Antarctic, *Deep Sea Res., Part II*, *58*(1–2), 74–83, doi:10.1016/j.dsr2.2010.05.024.
Hall, B. L., G. H. Denton, and B. Overturf (2001), Glacial Lake Wright, a high-level Antarctic lake during the LGM and early Holocene, *Antarct. Sci.*, *13*(1), 53–60, doi:10.1017/S0954102001000086.
Hoinka, K. P. (1985), What is a foehn clearance?, *Bull. Am. Meteorol. Soc.*, *66*(9), 1123–1132, doi:10.1175/1520-0477(1985)066<1123:WIAFC>2.0.CO;2.
Holland, P. R., H. F. J. Corr, H. D. Pritchard, D. G. Vaughan, R. J. Arthern, A. Jenkins, and M. Tedesco (2011), The air content of Larsen Ice Shelf, *Geophys. Res. Lett.*, *38*, L10503, doi:10.1029/2011GL047245.
Holland, P. R., A. Brisbourne, H. F. J. Corr, D. McGrath, K. Purdon, J. Paden, H. A. Fricker, F. S. Paolo, and A. H. Fleming (2015), Oceanic and atmospheric forcing of Larsen C Ice-Shelf thinning, *Cryosphere*, *9*(3), 1005–1024, doi:10.5194/tc-9-1005-2015.
Hosking, J. S., A. Orr, G. J. Marshall, J. Turner, and T. Phillips (2013), The Influence of the Amundsen–Bellingshausen Seas low on the climate of West Antarctica and its representation in coupled climate model simulations, *J. Clim.*, *26*(17), 6633–6648, doi:10.1175/JCLI-D-12-00813.1.
Jacobs, S. S., A. Jenkins, C. F. Giulivi, and P. Dutrieux (2011), Stronger ocean circulation and increased melting under Pine Island Glacier ice shelf, *Nat. Geosci.*, *4*(8), 519–523, doi:10.1038/ngeo1188.
King, J. C., and J. Turner (2009), *Antarctic Meteorology and Climatology*, Cambridge Univ. Press, Cambridge, U. K., doi:10.1017/CBO9780511524967.
King, J. C., T. A. Lachlan-Cope, R. S. Ladkin, and A. Weiss (2008), Airborne measurements in the stable boundary layer over the larsen ice shelf, Antarctica, *Boundary Layer Meteorol.*, *127*(3), 413–428, doi:10.1007/s10546-008-9271-4.
Kuipers Munneke, P., M. R. van den Broeke, J. C. King, T. Gray, and C. H. Reijmer (2012), Near-surface climate and surface energy budget of Larsen C ice shelf, Antarctic Peninsula, *Cryosphere*, *6*(2), 353–363, doi:10.5194/tc-6-353-2012.
Kwok, R., and J. C. Comiso (2002), Spatial patterns of variability in antarctic surface temperature: Connections to the southern hemisphere annular mode and the southern oscillation, *Geophys. Res. Lett.*, *29*(14), 1705, doi:10.1029/2002GL015415.
Liu, H., L. Wang, and K. C. Jezek (2006), Spatiotemporal variations of snowmelt in Antarctica derived from satellite scanning multichannel microwave radiometer and Special Sensor Microwave Imager data (1978–2004), *J. Geophys. Res.*, *111*, F01003, doi:10.1029/2005JF000318.
Long, D. G., and B. R. Hicks (2010), Standard BYU quikscat and seawinds land/ice image products, *Tech. Rep.*, BYU Center for Remote Sensing. Provo, Utah.
Lübbecke, J. F., N. J. Burls, C. J. C. Reason, and M. J. McPhaden (2014), Variability in the South Atlantic anticyclone and the Atlantic Niño mode, *J. Clim.*, *27*(21), 8135–8150, doi:10.1175/JCLI-D-14-00202.1.
Lubin, D., R. A. Wittenmyer, D. H. Bromwich, and G. J. Marshall (2008), Antarctic Peninsula mesoscale cyclone variability and climatic impacts influenced by the SAM, *Geophys. Res. Lett.*, *35*, L02808, doi:10.1029/2007GL032170.
Luckman, A., A. D. Elvidge, D. Jansen, B. Kulessa, P. Kuipers Munneke, J. King, and N. E. Barrand (2014), Surface melt and ponding on Larsen C Ice Shelf and the impact of foehn winds, *Antarct. Sci.*, *6*, 625–635.
Marshall, G. J. (2003), Trends in the southern annular mode from observations and reanalyses, *J. Clim.*, *16*(24), 4134–4143, doi:10.1175/1520-0442(2003)016<4134:TITSAM>2.0.CO;2.
Marshall, G. J., A. Orr, N. P. M. van Lipzig, and J. C. King (2006), The impact of a changing Southern Hemisphere annular mode on Antarctic Peninsula summer temperatures, *J. Clim.*, *19*(20), 5388–5404, doi:10.1175/JCLI3844.1.
Martin, P. J., and D. A. Peel (1978), The spatial distribution of 10 m temperatures in the Antarctic Peninsula, *J. Glaciol.*, *20*, 311–317.
Massom, R. A., et al. (2006), Extreme anomalous atmospheric circulation in the west Antarctic Peninsula region in austral spring and summer 2001/02, and its profound impact on sea ice and biota, *J. Clim.*, *19*(15), 3544–3571, doi:10.1175/JCLI3805.1.
Massom, R. A., S. E. Stammerjohn, W. Lefebvre, S. A. Harangozo, N. Adams, T. A. Scambos, M. J. Pook, and C. Fowler (2008), West Antarctic Peninsula sea ice in 2005: Extreme ice compaction and ice edge retreat due to strong anomaly with respect to climate, *J. Geophys. Res.*, *113*, C02S20, doi:10.1029/2007JC004239.
McGowan, H. A., D. T. Neil, and J. C. Speirs (2014), A reinterpretation of geomorphological evidence for Glacial Lake Victoria, McMurdo Dry Valleys, Antarctica, *Geomorphology*, *208*, 200–206, doi:10.1016/j.geomorph.2013.12.005.
Nicolas, J. P., and D. H. Bromwich (2014), New reconstruction of antarctic near-surface temperatures: Multidecadal trends and reliability of global reanalyses, *J. Clim.*, *27*(21), 8070–8093, doi:10.1175/JCLI-D-13-00733.1.
Nield, G. A., V. R. Barletta, A. Bordoni, M. A. King, P. L. Whitehouse, P. J. Clarke, E. Domack, T. A. Scambos, and E. Berthier (2014), Rapid bedrock uplift in the Antarctic Peninsula explained by viscoelastic response to recent ice unloading, *Earth Planet. Sci. Lett.*, *397*, 32–41.
Orr, A., G. J. Marshall, J. C. R. Hunt, J. Sommeria, C.-G. Wang, N. P. M. van Lipzig, D. Cresswell, and J. C. King (2008), Characteristics of summer airflow over the Antarctic Peninsula in response to recent strengthening of westerly circumpolar winds, *J. Atmos. Sci.*, *65*(4), 1396–1413, doi:10.1175/2007JAS2498.1.

Paolo, F. S., H. A. Fricker, and L. Padman (2015), Volume loss from Antarctic ice shelves is accelerating, *Science*, *348*, 327–331, doi:10.1126/science.aaa0940.
Parish, T. R. (1983), The influence of the Antarctic Peninsula on the wind field over the western Weddell Sea, *J. Geophys. Res.*, *88*(C4), 2684–2692, doi:10.1029/JC088iC04p02684.
Powers, J. G., A. J. Monaghan, A. M. Cayette, D. H. Bromwich, Y.-H. Kuo, and K. W. Manning (2003), Real-time mesoscale modeling over Antarctica: The Antarctic mesoscale prediction system, *Bull. Am. Meteorol. Soc.*, *84*(11), 1533–1545, doi:10.1175/BAMS-84-11-1533.
Pritchard, H. D., S. R. M. Ligtenberg, H. A. Fricker, D. G. Vaughan, M. R. van den Broeke, and L. Padman (2012), Antarctic ice-sheet loss driven by basal melting of ice shelves, *Nature*, *484*(7395), 502–505.
Rebesco, M., et al. (2014), Boundary condition of grounding lines prior to collapse, Larsen-B Ice Shelf, Antarctica, *Science*, *345*(6202), 1354–1358, doi:10.1126/science.1256697.
Rignot, E., G. Casassa, P. Gogineni, W. Krabill, A. Rivera, and R. Thomas (2004), Accelerated ice discharge from the Antarctic Peninsula following the collapse of Larsen B ice shelf, *Geophys. Res. Lett.*, *31*, L18401, doi:10.1029/2004GL020697.
Rignot, E., J. Mouginot, M. Morlighem, H. Seroussi, and B. Scheuchl (2014), Widespread, rapid grounding line retreat of Pine Island, Thwaites, Smith and Kohler glaciers, West Antarctica from 1992 to 2011, *Geophys. Res. Lett.*, *41*, 3502–3509, doi:10.1002/2014GL060140.
Scambos, T., C. Hulbe, and M. Fahnestock (2003), Climate-induced ice shelf disintegration in the Antarctic Peninsula, in *Antarctic Peninsula Climate Variability: Historical and Paleoenvironmental Perspectives*, edited by E. Domack et al., pp. 79–92, AGU, Washington, D. C., doi:10.1029/AR079p0079.
Scambos, T., H. A. Fricker, C.-C. Liu, J. Bohlander, J. Fastook, A. Sargent, R. Massom, and A.-M. Wu (2009), Ice shelf disintegration by plate bending and hydro-fracture: Satellite observations and model results of the 2008 Wilkins ice shelf break-ups, *Earth Planet. Sci. Lett.*, *280*(1–4), 51–60, doi:10.1016/j.epsl.2008.12.027.
Scambos, T. A., C. Hulbe, M. Fahnestock, and J. Bohlander (2000), The link between climate warming and break-up of ice shelves in the Antarctic Peninsula, *J. Glaciol.*, *46*(154), 516–530, doi:10.3189/172756500781833043.
Scambos, T. A., J. A. Bohlander, C. A. Shuman, and P. Skvarca (2004), Glacier acceleration and thinning after ice shelf collapse in the Larsen B embayment, Antarctica, *Geophys. Res. Lett.*, *31*, L18402, doi:10.1029/2004GL020670.
Scambos, T., T. Haran, M. Fahnestock, T. Painter, and J. Bohlander (2007), MODIS-based Mosaic of Antarctica (MOA) Data Sets: Continent-wide Surface Morphology and Snow Grain Size, *Remote Sens. Environ.*, *111*(2), 242–257, doi:10.1016/j.rse.2006.12.020.
Scambos, T. A., R. Ross, T. Haran, R. Bauer, D. G. Ainley, K. W. Seo, M. D. Keyser, A. Behar, and D. R. MacAyeal (2013), A camera and multisensor automated station design for polar physical and biological systems monitoring: AMIGOS, *J. Glaciol.*, *59*(214), 303–314, doi:10.3189/2013JoG12J170.
Schwerdtfeger, W. (1975), The effect of the Antarctic Peninsula on the temperature regime of the Weddell Sea, *Mon. Weather Rev.*, *103*(1), 45–51, doi:10.1175/1520-0493(1975)103<0045:TEOTAP>2.0.CO;2.
Schwerdtfeger, W. (1979), Meteorological aspects of the drift of ice from the Weddell Sea toward the mid-latitude westerlies, *J. Geophys. Res.*, *84*(C10), 6321–6328, doi:10.1029/JC084iC10p06321.
Skvarca, P., W. Rack, H. Rott, and T. I. Donángelo (1999a), Climatic trend and the retreat and disintegration of ice shelves on the Antarctic Peninsula: An overview, *Polar Res.*, *18*(2), 151–157, doi:10.1111/j.1751-8369.1999.tb00287.x.
Skvarca, P., W. Rack, and H. Rott (1999b), 34 year satellite time series to monitor characteristics, extent and dynamics of Larsen B Ice Shelf, Antarctic Peninsula, *Ann. Glaciol.*, *29*(1), 255–260, doi:10.3189/172756499781821283.
Skvarca, P., H. De Angelis, and A. F. Zakrajsek (2004), Climatic conditions, mass balance and dynamics of Larsen B ice shelf, Antarctic Peninsula, prior to collapse, *Ann. Glaciol.*, *39*(1), 557–562, doi:10.3189/172756404781814573.
Speirs, J. C., D. F. Steinhoff, H. A. McGowan, D. H. Bromwich, and A. J. Monaghan (2010), Foehn winds in the McMurdo Dry Valleys, Antarctica: The origin of extreme warming events, *J. Clim.*, *23*(13), 3577–3598, doi:10.1175/2010JCLI3382.1.
Speirs, J. C., H. A. McGowan, D. F. Steinhoff, and D. H. Bromwich (2013), Regional climate variability driven by foehn winds in the McMurdo Dry Valleys, Antarctica, *Int. J. Climatol.*, *33*(4), 945–958, doi:10.1002/joc.3481.
Steig, E. J., D. P. Schneider, S. D. Rutherford, M. E. Mann, J. C. Comiso, and D. T. Shindell (2009), Warming of the Antarctic ice-sheet surface since the 1957 International Geophysical Year, *Nature*, *457*(7228), 459–462, doi:10.1038/nature07669.
Steinhoff, D. F., D. H. Bromwich, and A. Monaghan (2013), Dynamics of the Foehn Mechanism in the McMurdo Dry Valleys of Antarctica from Polar WRF, *Q. J. R. Meteorol. Soc.*, *139*(675), 1615–1631.
Steinhoff, D. F., D. H. Bromwich, J. C. Speirs, H. A. McGowan, and A. J. Monaghan (2014), Austral summer foehn winds over the McMurdo dry valleys of Antarctica from Polar WRF, *Q. J. R. Meteorol. Soc.*, *140*(683), 1825–1837, doi:10.1002/qj.2278.
Tedesco, M. (2009), Assessment and development of snowmelt retrieval algorithms over Antarctica from K-band spaceborne brightness temperature (1979–2008), *Remote Sens. Environ.*, *113*(5), 979–997.
Thompson, D. W. J., and S. Solomon (2002), Interpretation of recent Southern Hemisphere climate change, *Science*, *296*(5569), 895–899, doi:10.1126/science.1069270.
Thompson, D. W. J., and J. M. Wallace (2000), Annular modes in the extratropical circulation. Part I: Month-to-month variability, *J. Clim.*, *13*(5), 1000–1016, doi:10.1175/1520-0442(2000)013<1000:AMITEC>2.0.CO;2.
Trusel, L. D., K. E. Frey, S. B. Das, P. K. Munneke, and M. R. Van Den Broeke (2013), Satellite-based estimates of Antarctic surface meltwater fluxes, *Geophys. Res. Lett.*, *40*, 6148–6153, doi:10.1002/2013GL058138.
Turner, J. (2004), The El Niño–Southern Oscillation and Antarctica, *Int. J. Clim.*, *24*(1), 1–31, doi:10.1002/joc.965.
Turner, J., G. J. Marshall, and T. A. Lachlan-Cope (1998), Analysis of synoptic-scale low pressure systems within the Antarctic Peninsula sector of the circumpolar trough, *Int. J. Clim.*, *18*(3), 253–280, doi:10.1002/(SICI)1097-0088(19980315)18:3<253::AID-JOC248>3.0.CO;2-3.
van den Broeke, M. (2005), Strong surface melting preceded collapse of Antarctic Peninsula ice shelf, *Geophys. Res. Lett.*, *32*, L12815, doi:10.1029/2005GL023247.
van Lipzig, N. P. M., G. J. Marshall, A. Orr, and J. C. King (2008), The relationship between the Southern Hemisphere Annular Mode and Antarctic Peninsula summer temperatures: Analysis of a high-resolution model climatology, *J. Clim.*, *21*(8), 1649–1668, doi:10.1175/2007JCLI1695.1.
Vaughan, D., G. Marshall, W. Connolley, C. Parkinson, R. Mulvaney, D. Hodgson, J. King, C. Pudsey, and J. Turner (2003), Recent rapid regional climate warming on the Antarctic Peninsula, *Clim. Change*, *60*(3), 243–274.
Zagorodnov, V., O. Nagornov, T. A. Scambos, A. Muto, E. Mosley-Thompson, E. C. Pettit, and S. Tyuflin (2011), Borehole temperatures reveal details of 20th century warming at Bruce Plateau, Antarctic Peninsula, *Cryosphere Discuss.*, *5*(6), 3053–3084, doi:10.5194/tcd-5-3053-2011.